7
Blue Phases

Peter P. Crooker

7.1 Introduction

Although liquid crystals have been known for more than 100 years, discovering the structures of their many thermodynamic phases is an activity that persists to this day [1]. The sheer variety has been impressive, including such novelties as uniaxial, biaxial, and ferroelectric fluids; phases with hexatic order; and chiral phases such as the blue phase (BP) and twist grain boundary (TGB) phase, which are stabilized by a lattice of defects. Many of these phases are unique in condensed matter physics; their presence never fails to challenge our notions of how matter can arrange itself in the aggregate.

This chapter reviews the present understanding of blue phases. Blue phases are distinct thermodynamic phases that appear over a narrow temperature range at the helical–isotropic boundary of highly chiral liquid crystals. In the absence of electric fields, there can be three blue phases: BPI and BPII, both of which have cubic symmetry; and BPIII, which possesses the same symmetry as the isotropic phase. Figure 7.1 shows schematically the phases in both *nonchiral* and *chiral* nematics. For nonchiral nematics, including racemic mixtures (with equal numbers of left- and right-handed versions of the same molecule) and even weakly chiral nematics, the nematic (or weakly chiral) phase heats directly to the isotropic phase. When the chirality is high, however, as many as three blue phases may appear.

An explanation of the nomenclature should be made here. First, chiral nematic molecules need not come from cholesteryl derivatives, so we use the term *chiral nematic* instead of *cholesteric* when referring to liquid crystal materials. The chiral nematic/cholesteric phase itself we will call *helical*. Second, blue phases got their name from their blue appearance in early investigations. Blue phases are not always blue, however; we now know that they may reflect light of other colors, including near infrared. Finally, BPIII was known as the fog phase or the gray fog phase in early publications. Although these terms are descriptive of this phase's appearance, BPIII seems to have survived.

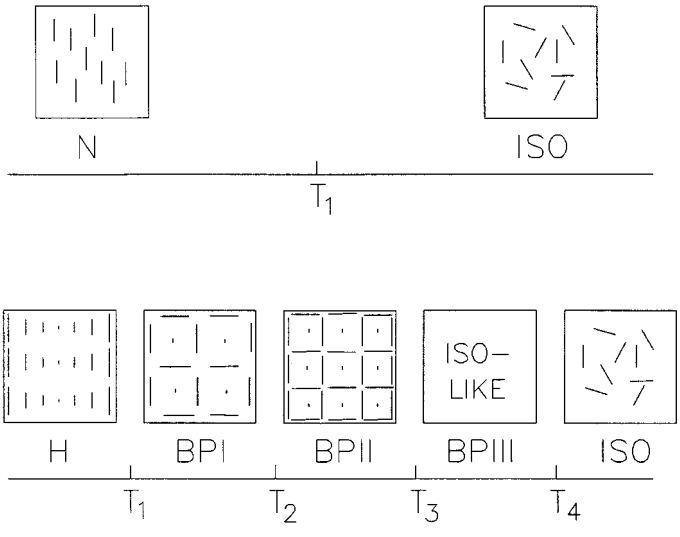

FIGURE 7.1. Schematic picture of the temperature region near the nematic (N)-isotropic (ISO) phase transition. Top: Nonchiral molecules have only nematic and isotropic phases. Bottom: Chiral molecules have helical (H) and isotropic phases, and, depending on the chirality, up to three blue phases (BPI, BPII, and BPIII). BPI and BPII are cubic; BPIII has the same symmetry as the ISO phase.

7.1.1 Chirality

That a liquid can have a cubic structure is truly remarkable. For a long time it was thought that a chiral nematic was just a nematic with twist, and that nothing fundamentally new was involved. As it turns out, this assumption was wrong. A nematic has orientational order, including mirror symmetry, but no positional order—it is invariant under a translation in any direction. When the nematic becomes chiral, the mirror symmetry is lost and the translational symmetry is reduced. Thus, in addition to becoming chiral, the chiral nematic also becomes spatially periodic.

The removal of mirror symmetry permits a chiral term, previously disallowed for nematics, to now be included in the Landau free energy [2], [3], [4]. The presence of this term greatly complicates minimization of the free energy in three dimensions and ultimately leads to the blue phases, which are periodic. (Interestingly, for a four-dimensional liquid crystal the minimization can be achieved [5], [6].) Chirality, therefore, leads to new phases and new physics.

The effect of adding periodicity to the nematic has been described by Brazovskii [7], [8]. The nematic–isotropic transition is an example of a transition between two *spatially uniform* phases, which means that the transition takes place at the origin of wave-vector space. Fluctuations of the system

away from the origin, which would add spatially periodic components to the structure, are energetically unfavorable and do not play a significant role in the transition. However, the isotropic–helical (or isotropic–blue phase) transition is an example of a transition between a uniform upper phase and a *spatially periodic* lower phase with spatial period P. Such a transition takes place on a spherical shell in **k**-space of radius $q_0 = 2\pi/P$. Fluctuations away from this shell are, as before, energetically unfavorable, but fluctuations along the surface of the shell, which merely alter the direction of the periodic axis, but do not change the magnitude of the free energy, are now allowed, with the result is that these fluctuations can significantly affect the nature of the transition. The chiral term therefore makes the helical/blue phase–isotropic transition fundamentally different from the nematic–isotropic transition, essentially by changing the topology of the minimal free energy surface in **k**-space. Other transitions affected by the Brazovskii mechanism are the smectic C–nematic transition and the Rayleigh–Benard instability in fluids.

7.1.2 Frustration

Another important feature of the blue phases is that of *frustration* [9], [10]. In frustrated systems, the conditions which produce a local energetic minimum cannot be extended globally. The blue phases are such systems; the lowest energy director configuration, as we will show later, is a cylindrical *double-twist* tube in which the director rotates spatially about any radius of a cylinder. Fitting these double-twist cylinders into a three-dimensional structure so that the directors match everywhere is topologically impossible, however, and so *disclinations*—line defects which appear where the cylinder directors cannot be matched—are necessary to relieve the elastic strain energy [11].

Figure 7.2 shows the situation for double-twist tubes with right-handed twist. If the tubes are stacked together to form a *left-handed* corner, the directors arrange themselves so that an $s = 1$ defect line is formed. The singularity can be removed, however, since all integer defect lines can escape. But the directors for a *right-handed* corner form an $s = -\frac{1}{2}$ defect. This singularity cannot be removed, since half-integer defect lines cannot escape. As we shall see, although the cubic blue phases can be described as lattices of double-twist tubes, frustration dictates that there also be an interpenetrating lattice of defects [12].

7.1.3 Defect-Mediated Melting

Defect theories of melting have been discussed in the context of crystal melting for some time [13]. In the usual three-dimensional defect melting theory, the free energy F_{def} for production of a defect out of a perfect crystal is calculated as a function of temperature. As the temperature increases, F_{def} is found to decrease smoothly from a positive to a negative value, passing

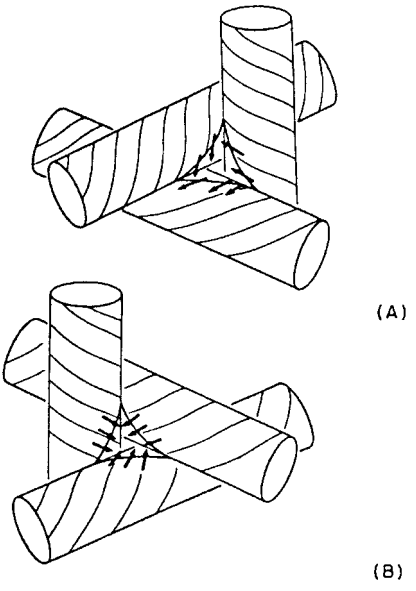

FIGURE 7.2. Stacking of double-twist tubes and frustration. The twist in each tube is taken to be right-handed, twisting to 45° at the tube boundary. (A) Right-handed corner: the directors form an $s = -\frac{1}{2}$ defect that cannot escape and is singular. (B) Left-handed corner: the directors form an $s = 1$ defect which *can* escape and is nonsingular. From Sethna [9].

through zero at some temperature T_c. Thus, below T_c defects are energetically unfavorable and the crystal is stable. Above T_c, however, defects are energetically *favorable*, a catastrophic onset of defects occurs, and the resulting liquid can be thought of as a solid saturated with defects.

Carrying this idea over to the helical–isotropic transition, there are two differences. First, we must use *disclinations*—topological line singularities in the director field of the liquid crystal—rather than crystal defects. The second difference is that the helical phase, which has no defects, "melts" to the blue phase, which is characterized by a stable *defect lattice* of line disclinations rather than by a random collection of defects. Indeed, there is more than one way to create such a lattice: thus BPI and BPII. The helical phase therefore melts to BPI, BPI melts to BPII, and, with a final onset of randomly positioned defects, BPII melts to the isotropic phase.

An intermediate phase consisting of a defect lattice is not an ingredient of the ordinary solid–liquid defect-melting scenario. It comes about because of liquid crystalline order and, as we shall see, the presence of high chirality.

7.1.4 Goal of This Review

A number of reviews of blue phases have already been written, notably those by Stegemeyer and coworkers [14], [15], Belyakov and Dmitrienko [16], Crooker [8], [17], Cladis [18], Seideman [19], and Wright and Mermin [20]. These reviews cover the experimental and theoretical work until 1989 when the cubic blue phases were most actively investigated. Since that time, effort

has been mainly directed toward understanding BPIII, although the cubic blue phases have not been ignored. This chapter will therefore discuss the early work rather quickly, the goal being to get to the more recent work. In particular, the emphasis will be more on experiment than theory, since the earlier theoretical reviews are quite extensive and contain much more mathematical detail than we care to reproduce here. Finally, the number of papers in the field has now grown quite large, and we despair of mentioning every work published. We will cover the main articles, however, and the reader should be able to obtain additional material from the references therein.

7.2 General Experimental Picture

Because the early blue phases were in cholesteryl esters and were difficult to see in a microscope, there was early skepticism over whether these phases existed at all. Now, as a result of thermal and optical observations, that doubt has been laid aside.

7.2.1 Thermal Data

The existence of three thermodynamically distinct blue phases is now firmly established by thermal, optical, and viscoelastic measurements. The initial experiments showed density discontinuities [21] and new peaks in differential scanning calorimetry traces [14], [22], [23], [24]. Additional evidence is found in viscoelastic data [25]. The most convincing proof, however, is revealed by heat capacity measurements [25], [26], [27]; those of Thoen [26] are shown in Figure 7.3. Here, in cholesteryl nonanoate, we see three peaks riding on the edge of the helical–isotropic peak; these peaks separate the helical, BPI, BPII, BPIII, and the isotropic phase. The sizes of the latent heats (in J mol^{-1}) are worth noting: Helical, 18; BPI, 5.8; BPII, 1.9; BPIII, 170; Iso. The value of 170 J mol^{-1} is typical for the nematic–isotropic transition; the blue phase transitions are less than a twentieth of that value. One can then argue that the order in the blue phases is consequently closer to the helical phase than to the isotropic phase, but as we shall see, that is only true for BPI and BPII. One might also conclude that BPII and BPIII are very similar since the latent heat between them is so small. In fact, we shall see that BPIII has much more in common with the isotropic phase.

7.2.2 Phase Diagrams

The easiest way to observe blue phases, provided their selective reflection wavelengths are in the visible wavelength region, is by polarized reflection microscopy. The visual appearance of the various textures is given by Crooker [17]. One would then like to see how the blue phases appear as a

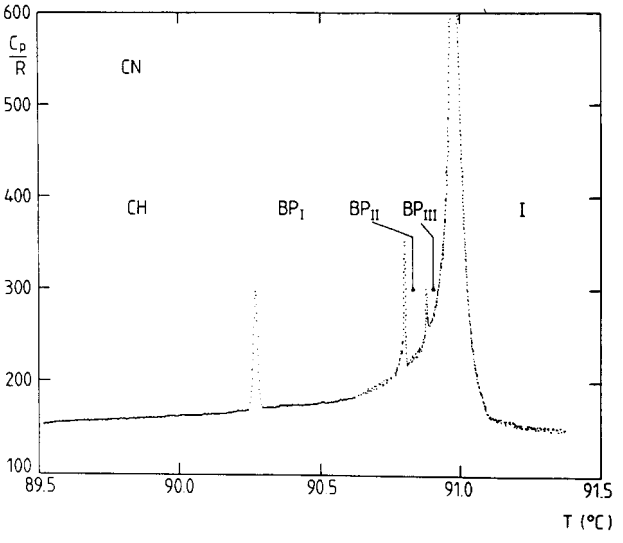

FIGURE 7.3. Heat capacity C_p/R versus temperature T in cholesteryl nonanoate (CN). Helical phase (CH), blue phases (BPI, BPII, BPIII), isotropic phase (I) (from Thoen [26]).

function of chirality $2\pi/P$, where P is the pitch. This can be achieved by mixing a chiral liquid crystal (enantiomer) with its racemate (a 50%–50% mixture of left- and right-handed enantiomers). Except for their chirality, the enantiomers are chemically identical and, to good approximation, may be mixed without changing the coefficients of the Landau free energy. For weight percent X of the pure enantiomer in a chiral–racemic mixture, $P = P_0/X$.

Figure 7.4 shows the phase diagram of CE2 (EM Chemicals), one of the most chiral liquid crystals available. Similar diagrams [28], [29], [30], [31] have shown that the blue phases always appear in the sequence BPI, BPII, and BPIII as the chirality is increased, and that, while BPI and BPIII appear to be increasingly stable at high chirality, BPII only exists over a limited region. Although BPIII is difficult to observe visually (the pitch of CE2 becomes so short that the selective reflections move into the ultraviolet), we shall discover later that the BPIII–isotropic coexistence line is first order, ending in a critical point at a higher chirality.

7.3 BPI and BPII—Theory

Research on blue phases has always been characterized by a close interplay between experiment and theory. The initial experiments were reported around 1979; in 1980, Hornreich and Shtrikman published the first Landau

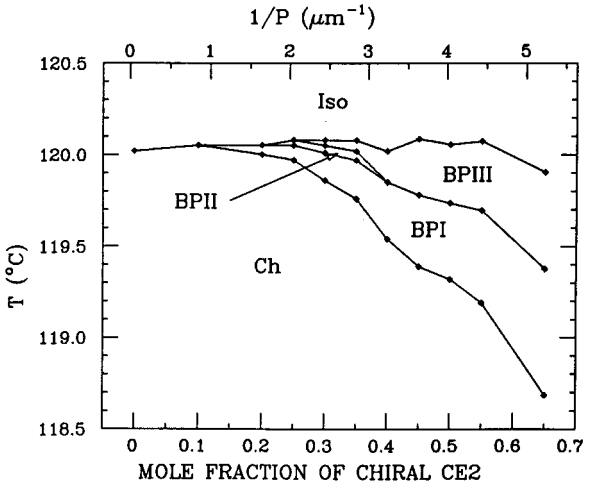

FIGURE 7.4. Transition temperatures T versus mole fraction chiral CE2 in a chiral–racemic mixture. The limited chirality range of BPII appears to be a universal feature of blue phases.

theory of a cubic blue phase [32]. This paper gave a tremendous boost to the field (although, astonishing to this reviewer, the theory seemed more credible to some than the experiments themselves!). Since that time, however, the theory has pointed the way to new experiments, while the experiments have suggested new avenues for theory. Here we concentrate on theories of the *cubic* blue phases—BPI and BPII. Only the main theoretical ideas are given; for more detail, we refer the reader to in-depth theoretical reviews and the references therein.

7.3.1 Landau Theory

A Landau theory for the cubic blue phases was first proposed by Brazovskii and Dmitriev [3], Hornreich and Shtrikman [32], [33], [34], [35], [36], [37], and Kleinert and Maki [38]. Detailed reviews of this approach have been given by Seideman [19], Belyakov and Dmitrienko [16], Wright and Mermin [20] and, in particular, by Hornreich and Shtrikman [39].

All Landau theories begin by first identifying an order parameter which incorporates the symmetry of the lower phase and which becomes zero in the upper phase. Next, a Landau free energy is constructed from the lowest powers of the order parameter, taking care to retain all terms allowed by symmetry and having a leading coefficient which is a linear function of temperature, passing through zero at some temperature T^*. Finally, the free energy is minimized with respect to the order parameter to find the structure. In the case of blue phases, however, the form of the free energy is sufficiently complicated that such a global minimization has not been possible. The

strategy has therefore been to compare the free energy of the isotropic phase with that of several proposed alternative structures to determine which one is most stable.

We first sketch out the theory without mathematical detail in order to give a general picture of the process. Let the order parameter be given by a symmetric, traceless tensor $\mathbf{Q}(\mathbf{r})$ which will just be the anisotropic part of the dielectric tensor. Since the Landau free energy is a scalar quantity, we expand it in lowest orders of scalar combinations of $\mathbf{Q}$. In very schematic form, this is just

$$F = \frac{1}{2}\int [a\mathbf{Q}^2 + c(\nabla\mathbf{Q})^2 - d(\nabla \times \mathbf{Q})\cdot\mathbf{Q} - \beta\mathbf{Q}^3 + \gamma\mathbf{Q}^4]\, d^3r, \tag{7.1}$$

where $a = \alpha(T - T^*)$ and α and the rest of the coefficients are constants. The coefficient d of the chiral term is proportional to the *chirality*. The terms of order $\mathbf{Q}^n$ give us the usual first-order nematic–isotropic transition; the $(\nabla\mathbf{Q})^2$ term represents the gradients in $\mathbf{Q}$ necessary to produce a cubic structure; and the $\mathbf{Q}\cdot(\nabla\times\mathbf{Q})$ term is a chiral term allowed because the molecules themselves lack mirror symmetry. It is this chiral term which greatly complicates the situation and causes the appearance of blue phases.

Since the anticipated cubic structure is periodic, we next expand $\mathbf{Q}(\mathbf{r})$ in a Fourier series with wave vector $\mathbf{k}$:

$$\mathbf{Q}(\mathbf{r}) = \sum_{\mathbf{k}}\sum_{m=-2}^{2} [Q_m(\mathbf{k})\mathbf{M}_m(\mathbf{k})]e^{i(\mathbf{k}\cdot\mathbf{r}+\psi_m(\mathbf{k}))}, \tag{7.2}$$

which says that each Fourier component of wave vector $\mathbf{k}$ has a *Fourier coefficient* given by the quantity in brackets and a *phase* given by $\psi_m(\mathbf{k})$. The coefficient has two parts. $\mathbf{M}_m(\mathbf{k})$ is the tensor part (because $\mathbf{Q}$ is a tensor) which gives the *director symmetry* of that particular Fourier component. Because the director symmetry is just that of the spherical harmonics $Y_{2m}(\theta,\phi)$, the $\mathbf{M}_m(\mathbf{k})$ tensors are represented by the Y_{2m}—one for each of the five values $m = 0, \pm1, \pm2$. The other part of the coefficient is a scalar, $Q_m(\mathbf{k})$, which represents the *amplitude* or *strength* of that particular Fourier component with symmetry $\mathbf{M}_m(\mathbf{k})$. The sum over m includes all the possible m values for a particular $\mathbf{k}$, while the sum over $\mathbf{k}$ includes all those wave vectors allowed by the symmetry of the system. In the isotropic phase, all $\mathbf{k}$ values are allowed. For the blue phase, however, one first chooses a particular unit cell to calculate, then allows only those values of $\mathbf{k}$, along with the accompanying phase factors $\psi_m(\mathbf{k})$, corresponding to the reciprocal lattice vectors (hkl) for that unit cell. For example, if the only nonzero coefficients $Q_m(\mathbf{k})$ are those corresponding to $\mathbf{k}$ vectors lying along the body-centered cubic (bcc) (110) directions, one finds that a structure with the bcc O^5 space group symmetry appears between the helical and isotropic phases. Allowing other coefficients to be nonzero will allow other structures to be tested which may or may not be more stable.

Substituting (7.2) in (7.1), one then adjusts the coefficients $Q_m(\mathbf{k})$ in order to minimize the free energy for the particular structure. A comparison of the free energies for this and other structures for various temperatures and chiralities then allows the construction of a temperature–chirality phase diagram.

Putting in some of the mathematical details [39], the Landau theory for the chiral nematic–isotropic transition has been described by de Gennes [2], who utilizes a tensor order parameter which is just the anisotropic part $\varepsilon_{ij}(\mathbf{r})$ of the total dielectric tensor $\varepsilon_{ij}^{d}(\mathbf{r})$:

$$\varepsilon_{ij}(\mathbf{r}) = \varepsilon_{ij}^{d}(\mathbf{r}) - \tfrac{1}{3}\mathrm{Tr}(\varepsilon_{ij})\delta_{ij}. \tag{7.3}$$

This tensor is symmetric, traceless, and will vanish in the isotropic phase.

The free energy includes the lowest-order scalar combinations of these tensors and their derivatives:

$$F = \int_V d^3r[\tfrac{1}{2}(a\varepsilon_{ij}^2 - 2de_{ijl}\varepsilon_{in}\varepsilon_{jn,l} + c_1\varepsilon_{ij,l}^2 + c_2\varepsilon_{ij,i}^2) - \beta\varepsilon_{ij}\varepsilon_{jl}\varepsilon_{li} + \gamma(\varepsilon_{ij}^2)^2]. \tag{7.4}$$

In this expression, the coefficients d, c_1, c_2, β, and γ are constants, while $a = \alpha(T - T^*)$ changes sign when $T = T^*$. The three terms with coefficients a, β, and γ are just those terms which appear in the nematic free energy; the c_1 and c_2 terms are order parameter gradients ($\varepsilon_{ij,l} = \partial\varepsilon_{ij}/\partial x_l$) which are also allowed for nematics. The chiral term with coefficient d is forbidden in nematics—it contains the antisymmetric tensor e_{ijl} and lacks nematic mirror symmetry.

This free energy is sufficient to treat the helical–isotropic transition, but due to the cubic term, global minimization is extremely difficult. In fact, there is no guarantee that the helical phase is the lowest energy phase available to nature. Hornreich and Shtrikman therefore propose other possibilities—cubic phases—and by comparing the resulting energies with the helical and isotropic energies are able to determine the most stable structure for given temperature and chirality.

In order to describe cubic phases, ε_{ij} is expanded in Fourier components as usual; but rather than allow *all* wave vectors, Hornreich and Shtrikman limit the expansion to just those wave vectors which correspond to the reciprocal lattice vectors of particular cubic space groups. The Fourier transform of $\varepsilon_{ij}(\mathbf{r})$ then takes the form

$$\varepsilon_{ij}(\mathbf{r}) = \sum_{h,k,l} N_{hkl}^{-1/2}\varepsilon_{ij}(h,k,l)e^{ik_{hkl}(hx_1 + kx_2 + lx_3)}. \tag{7.5}$$

Thus a particular cubic structure is characterized by reciprocal lattice vectors $\mathbf{k}_{hkl}$ with Miller indices (h,k,l), and there are N_{hkl} reciprocal lattice vectors of length k_{hkl}.

The $\varepsilon_{ij}(h,k,l)$ tensor consists of the Cartesian representations of the spherical harmonics $Y_{2m}(\theta,\phi)$. Schematically,

$$\varepsilon_{ij}(h,k,l) = \sum_{m=-2}^{2} \varepsilon_{m,hkl} e^{i\psi_{m,hkl}} [M_{m,hkl}] \tag{7.6}$$

$$= \varepsilon_0 e^{i\psi_0} \begin{pmatrix} -1 & 0 & 0 \\ 0 & -1 & 0 \\ 0 & 0 & 2 \end{pmatrix} + \varepsilon_1 e^{i\psi_1} \begin{pmatrix} 0 & 0 & 1 \\ 0 & 0 & i \\ 1 & i & 0 \end{pmatrix} + \text{c.c.} + \varepsilon_2 e^{i\psi_2} \begin{pmatrix} 1 & i & 0 \\ i & -1 & 0 \\ 0 & 0 & 0 \end{pmatrix} + \text{c.c.} \tag{7.7}$$

Here c.c. means complex conjugate; also we have left out some numerical coefficients and suppressed the indices hkl on ε_m, ψ_m, and M_m. The basis matrices are defined in a local right-handed coordinate system for each $\mathbf{k}_{hkl}$. Thus, for any particular wave vector $\mathbf{k}_{hkl}$ there may be as many as five different Fourier components ($m = 0, \pm 1, \pm 2$), each having a *director symmetry* specified by M_m, an *amplitude* given by ε_m, and a *phase* by ψ_m.

The remaining strategy is then to decide on a particular space group to describe, write down the appropriate Fourier components and their phases ab initio, then determine the magnitude of the coefficients by numerical minimization of the free energy. This process leads to cubic structures through the following reasoning: Since the minimization involves the cubic term, one seeks contributions from wave-vector triads whose vector sum is zero, that is, a triangle of wave vectors. Selection of wave vectors with $m = 2$ symmetries will also minimize the quadratic part of the free energy. The simplest three-dimensional structure is obtained by choosing a set of wave vectors forming the six edges of a regular tetrahedron. The result is a body-centered cubic (bcc) structure with the space group O^5 ($I432$).

Utilizing this basic tetrahedron of wave vectors and adding *harmonics*, Hornreich and Shtrikman have been able to construct other bcc structures, along with simple cubic (sc) and face-centered cubic (fcc) structures. The next step is therefore to construct a phase diagram showing that particular structure which minimizes the free energy at each point of the temperature–chirality plane. An example of such a phase diagram is given in Figure 7.5, which shows temperature t and chirality κ in nondimensional, reduced units. The various phases represented are the usual isotropic (I) and helical (C) phases, plus cubic blue phases, with space groups given by bcc O^5 ($I432$), bcc O^8 ($I4_132$), and sc O^2 ($P4_232$).

The big success of this theory is that cubic phases are shown to indeed be more stable than the helical phase at the helical–isotropic boundary.

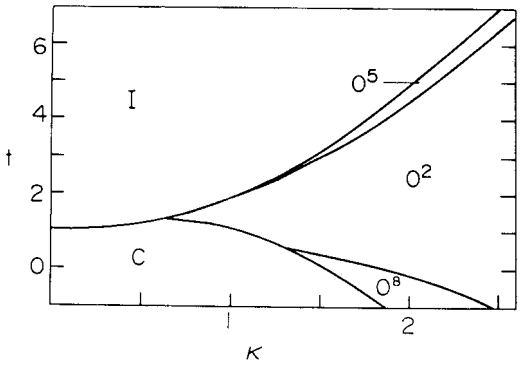

FIGURE 7.5. Theoretical phase diagram from the Landau theory with higher harmonics. Temperature t and chirality κ are in reduced units. The helical (C), isotropic (I), and cubic (O^2, O^5, O^8) phases are allowed. From Grebel et al. [37]. This figure should be compared with Figure 7.4.

Furthermore, both bcc and sc structures have been found, which agrees with experimental findings. Comparison of Figure 7.5 with Figure 7.4, however, reveals that the experimental and theoretical phase diagrams differ considerably in detail—not only quantitatively, but qualitatively as well. Finally, the analysis presented here only predicts the cubic BPI and BPII phases. Despite attempts, the noncubic BPIII phase does not come out of the analysis.

Extensions of the Landau theory are possible, for example, by introducing higher-order elastic terms in (7.2) as has been done by Longa et al. [40]. The resulting phase diagrams are richer, but still differ from the experimental phase diagrams.

7.3.2 *Defect Theory*

The fundamental cause of macroscopic chirality in liquid crystals is that the molecules themselves are chiral. Consequently, the interactions between adjacent molecules are also chiral: twist arises because the interaction energy of two adjacent molecules is minimized when they are at a slight angle to each other. In the conventional helical phase, this condition is only partially met—twist occurs along the single axis **k** but not along axes perpendicular to the twist axis. Clearly, the energy can be further lowered by allowing twist in all directions perpendicular to the local director. Such a configuration, called *double twist*, is shown in Figure 7.6. It has been shown that a tube of double twist does indeed have lower free energy than the conventional, single-twist helical structure, but only near the axis [1], [9]. If the local twist becomes as much as 90°, substantial bend distortion occurs and the energy advantage is lost. Consequently, the twist in a tube is limited to 45°. One can then envision assembling double-twist tubes in a regular lattice having the space group symmetries discussed above, filling the interstices with nematic material, and allowing the directors to relax everywhere to achieve equilibrium.

If such a program is carried out, the intersections between double-twist tubes can be shown to have incompatible directors, which leads in turn to *frustration* and the introduction of *disclinations*, as described earlier [9].

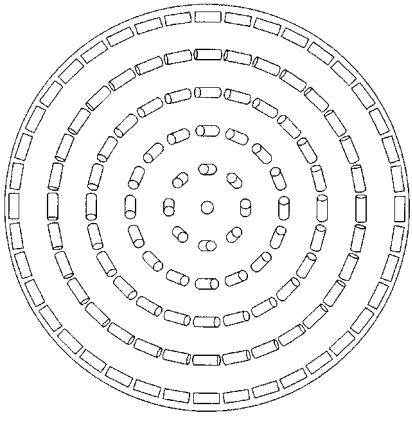

FIGURE 7.6. Cross-sectional view of a double-twist region. The director is parallel to the tube axis at the center, twisting along any radius. The energy of such a configuration is lower than for twist in a single direction, but only near the center. In a double-twist tube, the angle at the edge is $\approx 45°$.

One can think of the blue phase as a lattice of double-twist tubes (which necessitates a lattice of disclinations) or a lattice of disclinations (which necessitates a lattice of double-twist tubes) [20]. Thus, a theory involving a lattice of double-twist tubes becomes implicitly a theory for a lattice of defects.

The defect theory of blue phases was initially introduced by Meiboom, Sethna, Anderson, and Brinkman [5], [6], [12], [41], [42], [43]. For detailed reviews see Sethna [9] and Wright and Mermin [20].

Calculating the free energy for a lattice of defects is a difficult task. Meiboom et al. [12] start by writing the free energy per unit length F_{disc} of a single disclination line, which consists of four terms:

$$F_{\text{disc}} = F_{\text{el}} + F_{\text{surf}} + F_{\text{core}} + F_{\text{int}}. \tag{7.8}$$

The first term is the elastic energy associated with the defect, which has the form

$$F_{\text{el}} \sim K \ln(R_0/R_c). \tag{7.9}$$

This term comes from calculating the usual Frank free energy (i.e., with bend, twist, and splay, and equal elastic constants) outside a disclination core of radius R_c but inside a cutoff radius size R_0.

The second term is an additional elastic term

$$\begin{aligned} F_{\text{surf}} &= \frac{1}{2}\int K\nabla \cdot [(\mathbf{n}\cdot\nabla)\mathbf{n} - \mathbf{n}(\nabla\cdot\mathbf{n})]\, d^3r \\ &\sim -K, \end{aligned} \tag{7.10}$$

which is usually dropped because it transforms to a surface integral. In this case, however, the integral must also be taken over the inner surface of the defect core and cannot be ignored. This is, in fact, the term that pulls the energy of the defect below zero.

The third term

$$F_{\text{core}} = \alpha(T_{\text{iso}} - T)\pi R_0^2, \tag{7.11}$$

arises because the energy cost of maintaining a highly strained, nonzero order parameter at the core is greater than the energy required to drive the core itself isotropic, even though the temperature is below the usual helical–isotropic transition temperature T_{iso}. The quantity $\alpha(T_{\text{iso}} - T)$ is just the difference between the free energies of the isotropic and helical phases.

Finally, the last term

$$F_{\text{int}} = 2\pi\sigma R_c, \tag{7.12}$$

is an interfacial energy, characterized by surface tension σ, between the core and the chiral material outside. Its importance is probably minor.

Summing all these terms, it is easy to see that the free energy is positive for T far enough below T_{iso}, but may become negative for temperatures close to, but still less than, T_{iso}. This feature opens the possibility for a transition to a blue phase lattice just below T_{iso}.

The strategy is to assemble a lattice of defects having a particular space group symmetry and fill the interstices with nematic material. The director is then allowed to relax everywhere (except of course at the defects) and the free energy calculated. From this process one finds that there is also an interpenetrating lattice of double-twist tubes and that the whole structure is stable between the helical and isotropic phases. Figure 7.7 shows both the double-twist lattice and the defect lattices for the proposed structures sc O^2 and bcc O^{8-}. Other structures—bcc O^5 and bcc O^{8+}—have also been worked out [42].

7.3.3 *Comparison of the Landau and Defect Theories*

The Landau theory uses an order parameter with cubic symmetry which is relaxed over a cubic unit cell in order to determine the minimum free energies of various structures. The defect theory utilizes an assumed lattice of defects and allows director orientations to conform to this lattice. Wright and Mermin [20] have argued that the Landau theory is therefore a "high chirality" model, while the defect theory describes "low chirality." Despite these differences, however, the Landau and defect theories have many similarities. Both theories result in double-twist regions, which are fitted together to form three-dimensional structures. Both theories also include defects—in the defect theory they are explicit disclination lines where the order parameter goes to zero abruptly; in the Landau theory, they appear implicitly as regions where the order parameter becomes zero gradually. To describe these defects in Fourier space, the defect theory would require many higher-order, spatial Fourier components. The Landau theory, on the other hand, uses very few Fourier components. Thus, the main difference between the Landau and defect theories may just be the number of Fourier compo-

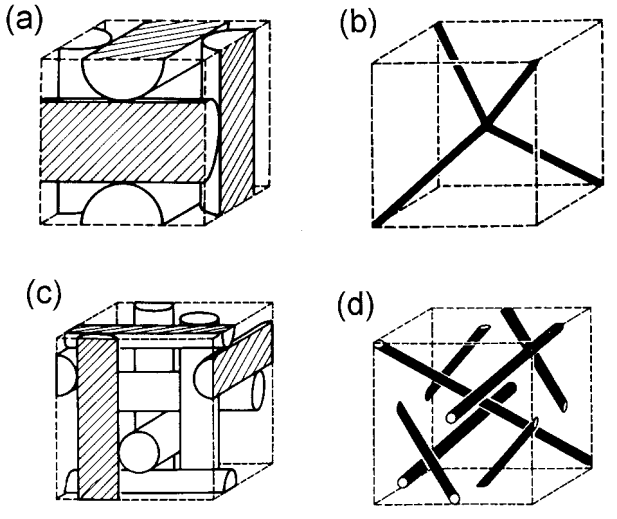

FIGURE 7.7. Models of cubic blue phases. (a) Arrangement of double-twist tubes for the sc O^2 structure. (b) Corresponding unit cell of defect lines for the sc O^2 structure. (c) Arrangement of double-twist tubes for the bcc O^{8-} structure. (d) Unit cell of defect lines for the bcc O^{8-} structure. From Dubois-Violette and Pansu [10].

nents included in the order parameter rather than any fundamental differences in the structures.

For excellent discussions of the blue phases from the viewpoint of geometry, topology, and frustration, the articles by Dubois-Violette and Pansu [10] and Pansu [44] are recommended.

7.3.4 *The Bond-Orientational Order and Fluctuation Models*

In any theoretical model of the cubic blue phases, a meeting point with experiment should be a comparison of theoretical and experimental phase diagrams. Despite theoretical successes, however, the theoretical phase diagrams (Figure 7.5) are still missing essential features of the experimental phase diagrams (Figure 7.4). The missing features are:

- Theory has correctly predicted the space groups of the helical, BPI, and BPII phases, and their order with increasing temperature is theoretically correct. The theoretically predicted bcc O^5 phase, however, has never been detected experimentally.
- In the theoretical phase diagrams, the BPII region becomes broader with increasing chirality. Experimentally, however, BPII vanishes at high chirality.
- The theoretical phase diagrams do not reproduce the experimentally observed BPIII phase.

- The theoretical phase diagrams do not reproduce the experimentally observed critical point which terminates the BPIII–isotropic coexistence line at high chirality.

The cubic bond-orientational order (BOO) model of Trebin and coworkers [45], [46] is an attempt to rectify these theoretical problems. Originally formulated for crystals, the central idea of BOO is that the *positional* order of the atoms can be lost (due to formation of defect pairs or fluctuations) while still retaining the *orientational* order of the bonds. An analogous situation would occur for a floor loosely tiled with square tiles. If the sides of the tiles are all aligned properly, but the tiles are not fitted together correctly, orientational order is retained while positional order is lost.

In the blue phases, the atoms and bonds are replaced by the unit cell's corners and edges, respectively. The goal of the BOO model of blue phases is to convert the higher temperature O^5 phase to a cubic phase with only bond-orientational order, which might then be the amorphous-appearing BPIII. The authors accomplish this by adding a fluctuational term to the usual Landau free energy, the minimization of which leads to various phase diagrams depending on the coupling strength. These phase diagrams have the required BOO phase just below the isotropic phase, but the O^5 itself is not completely destabilized. Nevertheless, the authors claim that the BOO phase would be a likely candidate for BPIII.

With the realization that the BPIII–Iso transition ended in a critical point, Trebin and coworkers [47] have also proposed a fluctuation-dominated model of the blue phases. Here the order parameter coefficient is separated into a nonfluctuating term and a fluctuating term and the free energy accordingly separated into a mean-field and a fluctuating part. On the one hand, the resulting phase diagrams are encouraging: the O^5 phase does not appear (but only for large transition temperatures) and BPII disappears at high chirality. On the other hand, a simplification of the theory provides only "a hint of the occurrence of a second isotropic phase [i.e., BPIII] and of a critical point at high chiralities" [47].

7.4 BPI and BPII—Experiment

A number of experimental techniques have been used to elucidate the structure of BPI and BPII. In what follows, we will summarize them and show how the accumulated experimental evidence gives us a good picture of these phases.

7.4.1 Bragg Scattering

It is well known that the helical phase with a planar texture will selectively reflect light. Selective reflection requires light which has a circularly polar-

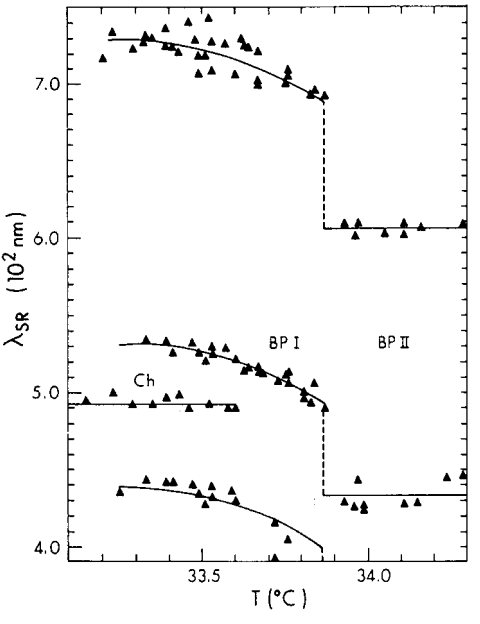

FIGURE 7.8. Selective reflection wavelengths λ_{SR} versus temperature for a mixture of chiral CB15 and nematic E9. Note that BPI supercools into the helical (Ch) phase, whereas the BPI–BPII transition is reversible. The ratios of the wavelengths are those for simple cubic or body-centered cubic lattice symetry (from Johnson, Flack, and Crooker [54]).

ized component with the same handedness as the helix and a wavelength satisfying $\lambda = nP$, where n is an average refractive index and P is the pitch. In the cubic blue phases, however, there may be several selective reflection wavelengths corresponding to various crystal planes, none of which coincide with the helical selective reflection wavelength. Initial reporting of this effect was by Stegemeyer and coworkers [14], [48], [49], [50], [51]. In a related experiment, Meiboom and coworkers [42], [52], [53] measured the *transmitted* light through an unaligned blue phase sample. Such a measurement yields a step in the transmitted intensity at each selective reflection wavelength.

The selective reflection wavelengths of a mixture of chiral CB15 and nematic E9 (both obtained from BDH Chemicals) are shown in Figure 7.8 [54]. In both BPI and BPII, the wavelengths have the ratios λ_0, $\lambda_0/\sqrt{2}, \lambda_0/\sqrt{3}, \ldots$, where λ_0 is the longest selective reflection wavelength. These ratios are well known from X-ray diffraction: they are the signature of Bragg scattering from either a body-centered cubic (bcc) or simple cubic (sc) lattice. The conclusion, then, is that BPI and BPII are cubic, but with lattice parameters of the order of visible light wavelengths. Furthermore, as can be seen in Figure 7.8, the lattice parameters of BPI and BPII are different. One then wonders whether the lattice structures are also different.

To distinguish bcc from sc, Hornreich and Shtrikman [55], [56] and Belyakov et al. [57] worked out the polarization selection rules for each possible sc and bcc space group. As shown in (7.7), each set of Bragg planes contains five order parameter coefficients—$\varepsilon_0, \varepsilon_{\pm 1}$, and $\varepsilon_{\pm 2}$—each of which

reflects circularly polarized light (rcp or lcp polarizations) in a unique way. In particular, the third line of the sc lattice [sc (111)] should reflect circularly polarized light as an ordinary mirror (rcp $\rightarrow$ lcp, lcp $\rightarrow$ rcp), whereas the third bcc line [bcc (211)] should reflect only that polarization corresponding to the twist of the helix (rcp $\rightarrow$ rcp, lcp $\rightarrow$ no reflection). However, experiments relying on this technique [58] give results which violate these rules and are in conflict with other methods, namely platelet growth morphology and Kossel diagrams. Despite efforts to resolve the selection rule contradiction [59], [60], the latter techniques have proved a more reliable way of identifying structures.

Another way to identify the dominant contributions of the order parameter for a particular line, is to experimentally determine the reflecting Mueller matrix of the Bragg-reflecting blue phase. The polarizations of light incident and scattered from a surface can be described by four-component Stokes vectors. The matrix which transforms one to the other (and describes the blue phase) is a 4×4 Mueller matrix. By analyzing the reflected Stokes vectors for a range of incident Stokes vectors, the complete Mueller matrix can be determined. The result of such measurements [61], [62] was that the ε_{-2} coefficient completely dominates the other coefficients, which rules out certain space groups.

7.4.2 Kossel Diagrams

A specialized case of Bragg scattering is the Kossel diagram technique, first used for blue phase analysis by Pieranski and coworkers [63], [64], [65], [66] and more recently by Miller and Gleeson [67], [68]. Figure 7.9 illustrates the basic principle [68]. The blue phase sample S, with one of the sets of crystal planes shown, is illuminated with highly convergent light through microscope objective L. If the light is monochromatic with wavelength λ/n in a material with crystal planes separated by distance d, a particular cone of the incident rays will satisfy the Bragg condition $\lambda = 2nd\sin(\theta)$. This cone of rays is backscattered, refocused through the objective, and brought to an image in the back focal plane FP of the objective. Examination of this plane reveals the Kossel diagram, in which each of the sets of crystallographic planes in the sample is projected on the back focal plane as a circle or an ellipse. Without further analysis, it is clear that the symmetry of the Kossel diagram is just the symmetry of the crystal itself. Thus, the longest wavelength bcc line [bcc (110)] and the longest wavelength sc line [sc (100)] can be distinguished because only the sc (100) Kossel line has fourfold symmetry. In addition, quantitative measurements of the Kossel diagrams allows the angles and crystal-plane spacing to be determined. This method has proven to be of great utility in characterizing the electric-field-induced BPX phase and in determining that the symmetry of BPII is sc O^2 ($P4_232$).

More recently, Kossel diagrams have been utilized by Miller, Gleeson, and Lydon [69] to address the well-known "phase problem"—that is, to

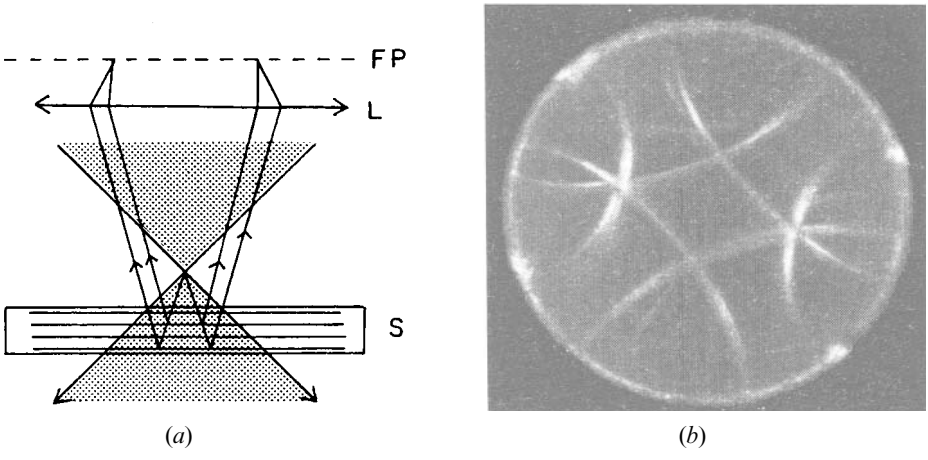

(*a*) (*b*)

FIGURE 7.9. Principle of the Kossel diagram technique. (a) From the cone of incident monochromatic light, sets of crystal planes in sample S Bragg scatter light back through the objective lens L to make a Kossel diagram at focal plane FP. (b) Each set of planes is represented by an arc in the Kossel diagram (Kossel diagram courtesy of B. Jérôme).

determine the relative phases of the Bragg reflections. This phase determination is achieved by examining the regions where two Kossel rings either intersect or pass close to each other. Interference fringes are observed experimentally, and when these fringes are modeled by a simple theory, they are seen to depend sensitively on the phase shift between the lattice planes causing the respective rings. Figure 7.10 shows experimental and theoretical results from two Kossel rings intersecting perpendicularly; note the presence of gaps in the lines near the intersection. In particular, the (100) and (010) planes of BPII have been examined, which, according to the double-twist

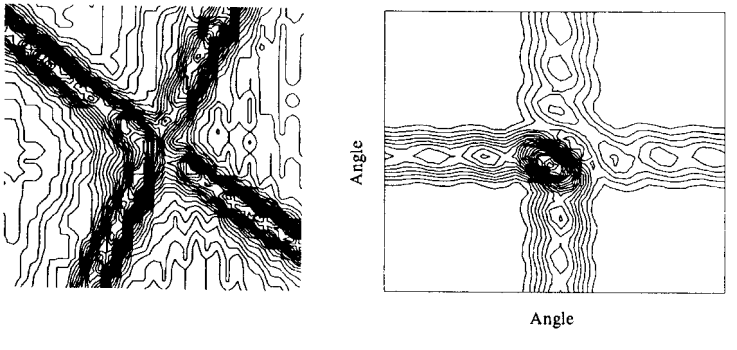

FIGURE 7.10. Interference patterns for Kossel lines intersecting at right angles. Left: experiment. Right: theory (from Miller et al. [69]).

model (see Figure 7.7), should have a relative phase shift of π. The data do not account for this phase shift, however, and hence details of the BPII structure remain unresolved.

7.4.3 Crystallite Morphology

Much of the original information on blue phases was deduced from microscopic examination of the textures [70], [71]. Electron microscopy of freeze-fractured samples has also been performed, but the results are difficult to interpret [72], [73].

A more reliable and direct way to determine a crystal's space group is to carefully grow the crystal and observe its shape, which has the same symmetry as the unit cell. It is possible to do this in the two-phase region of a multicomponent mixture, and/or in a temperature gradient. Contributors to this effort have been primarily Stegemeyer and coworkers [74], [75], [76], [77], [78] and Pieranski and coworkers [79], [80], [81], [82]. See also the review by Stegemeyer [15]. Figure 7.11 is an example of such a crystallite in BPI. From pictures like these, along with Kossel diagram information, it has been determined that BPI is body-centered cubic with space group O^8 ($I4_132$), and BPII is simple cubic with space group O^2 ($P4_232$). Both of these space groups are shown to be stable in the Hornreich and Shtrikman [39] theory.

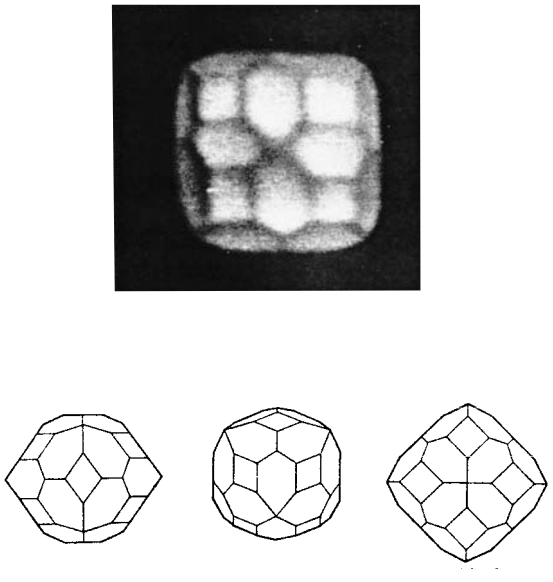

FIGURE 7.11. BPI crystallite. Top: Microscope picture, viewed along the (200) axis. Bottom: From left to right, views along the (110), (211), and (200) axes (from Barbet-Massin, Cladis, and Pieranski [79]).

7.4.4 Rotatory Power

The experimental signature of a chiral structure is rotatory power, in which the plane of polarization of a beam of linearly polarized light is rotated after passing through a chiral sample. The earliest rotatory power measurements established the chiral nature of the BPI and BPII blue phase peaks [48], [49], [83]. Later measurements have followed and have even been able to provide values of the order parameters [84], [85], [86], [87]. Theories for the behavior have been provided by Bensimon et al. [88] and Belyakov et al. [84]. The biggest utility of rotatory power, however, has been in elucidating the nature of BPIII, as we shall see below.

7.4.5 Viscoelastic Measurements

An important question to ask of blue phases is whether they are liquid or solid. The cubic structure is not one of atoms in fixed positions as in a conventional crystal—rather, the molecules are free to diffuse randomly throughout the blue phase lattice, changing their orientation en route so as to conform to the blue phase's spatially dependent order.

Solids are characterized by a nonzero static shear elastic constant, whereas a liquid will not support static shear. Conventional viscometric techniques (i.e., capillary flow and falling balls), which now seem rather crude considering the fragile nature of the blue phase lattice, initially showed a large viscosity peak at the helical–isotropic transition [89], [90], [91]. Viscosities and other transport coefficients associated with the pretransitional region of the isotropic phase were addressed by light scattering [92], [93], [94], [95].

Once the cubic nature of the blue phase was established, attempts to measure the elastic constants using more sensitive techniques appeared shortly thereafter [25], [96], [97], with those of Kleiman et al. [25] being the most extensive. The latter experiments are very delicate, since the blue phase lattice is both soft (small elastic constants) and weak (small elastic limit). Torsional oscillators configured as cup viscometers were used and the shear distortion was kept to less than 0.02%. Figure 7.12 shows results for both the shear elasticity G and the viscosity η. These data are taken at various frequencies and must be extrapolated to 0 Hz to obtain the static properties. In the helical phase the extrapolation is somewhat dependent on the model; nevertheless, the authors claim that G becomes *nearly* zero in the helical phase and about 710 dyn cm^{-2} in BPI. (This figure should be compared to $\sim 10^{11}$ dyn cm^{-2} in a metal!) However, since BPI also possesses viscosity, its behavior is that of a viscoelastic solid.

Another way to assess the elastic constants in the blue phases is to observe their behavior in the Cano wedge configuration, which tends to compress and stretch the blue phase lattice parameter. This strain also raises the free energy and alters the blue phase transition temperatures, as has been shown by Feldman et al. [98]. For more discussion of blue phases in the Cano wedge configuration, see the papers by Stegemeyer and coworkers [99], [100].

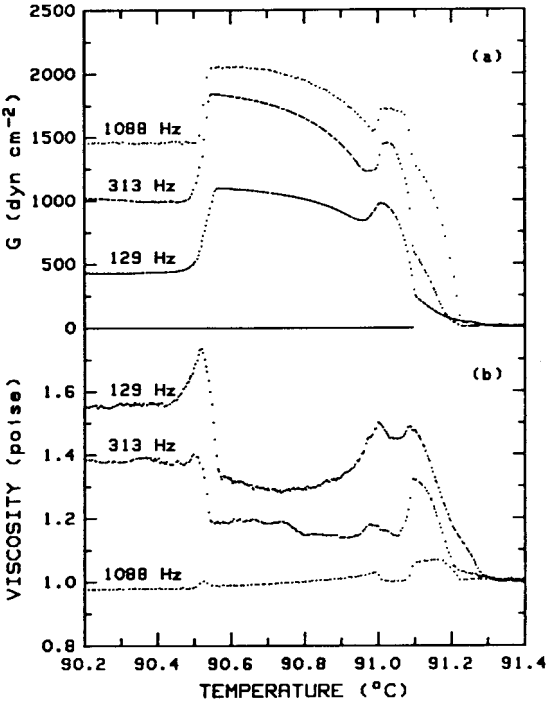

FIGURE 7.12. (a) Shear elastic constant and (b) viscosity for cholesteryl nonanoate for different frequencies (from Kleiman et al. [25]).

7.5 Electric Field Effects

When electric fields are applied to liquid crystals, the molecules tend to align—either parallel to the field (for $\varepsilon_a > 0$) or perpendicular (for $\varepsilon_a < 0$). For the case of nematics, which already have a preferred direction, the director is simply reoriented without breaking the symmetry. However, the helical phase has two nonequivalent directions: the twist axis, and the director, which rotates spatially about the twist axis. If $\varepsilon_a > 0$, such a helical director is clearly incompatible with a uniform field. For this case, an increasing field first distorts the helix, then stretches out the pitch, and finally causes the well-known cholesteric–nematic transition [1]. If $\varepsilon_a < 0$, the helical director is only compatible with a uniform field if the twist axis and field are parallel.

Since the cubic blue phases have three equivalent axes, an applied field breaks the cubic symmetry and creates a preferred axis. But, like the helical phase, blue phases are chiral, being composed of a lattice of double-twist tubes. It is therefore not surprising that applied fields lead to distortion of the lattice (electrostriction) and, for high enough fields, new lower-symmetry phases. These effects occur for both $\varepsilon_a < 0$ and $\varepsilon_a > 0$.

Electric field effects on blue phases have been reviewed previously by

Kitzerow [101]. Since electric field-induced phases were studied first, we describe them next. Electrostriction of blue phases will then be discussed at the end of this section.

7.5.1 *Electric Field-Induced Phases*

The first experiments with electric fields showed that an increasing field initially lengthens the blue phase lattice parameter and causes birefringence. A theory for weak fields was given by Lubin and Hornreich [102]. With larger fields, the blue phases may transform between themselves, to the helical phase, and ultimately to the nematic phase [23], [103], [104], [105], [106], [107], [108], [109]. Fields also affect the orientation and facetting of blue phase crystallites [81], [82], [110].

At the same time, Hornreich, Kugler, and Shtrikman [111], [112] predicted from Landau theory that a two-dimensional hexagonal blue phase, BPH^{2D}, should be stabilized by an electric field when the dielectric anisotropy is positive ($\varepsilon_a > 0$). This prediction led to a search for other blue phase structures. Subsequent temperature–electric field phase diagrams [113], [114] showed that other phases did in fact occur, but identification of the new structures was much more difficult. Figure 7.13, due to Porsch and Stegemeyer [113], shows a CB15/E9 mixture in which a new phase, BPE, is detected. Figure 7.14, due to Pieranski et al. [115], shows the same material and identifies hexagonal platelets found by growing crystallites in the BPII–isotropic two-phase region. The presence of hexagonally shaped crystallites was the first reliably identifiable hexagonal phase.

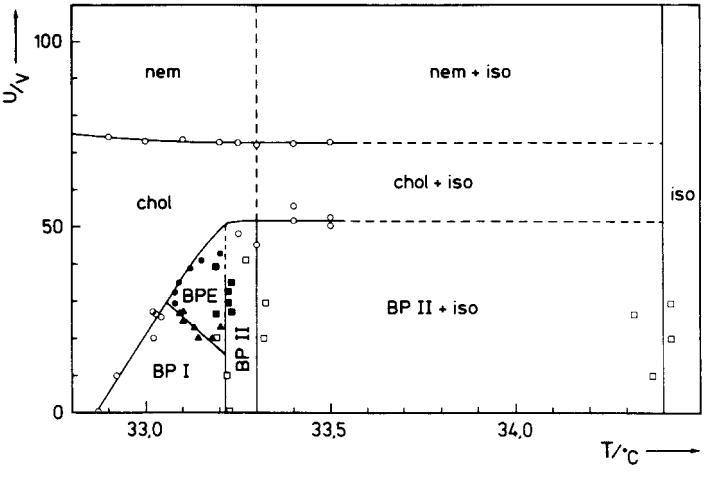

FIGURE 7.13. Voltage–temperature phase diagram for a 49.6% mixture of chiral CB15 nematic E9. The helical phase is labeled "chol"; the structure BPE was not yet determined in this article (from Porsch and Stegemeyer [113]).

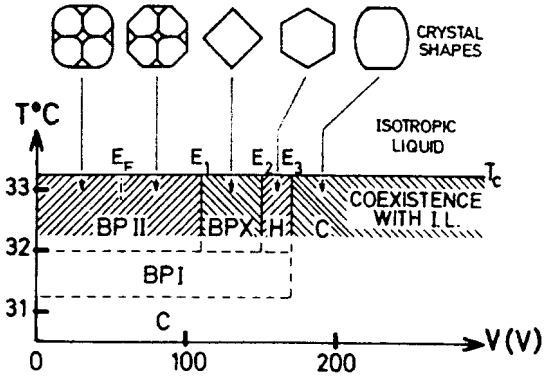

FIGURE 7.14. Schematic voltage–temperature phase diagram for a 49.8% mixture of CB15 in E9. The shaded region is the coexistence region in which crystals of different shapes appear. C is the helical phase; H is the hexagonal BPH^{3D} phase (from Pieranski et al. [115]).

This hexagonal phase was not, however, the predicted BPH^{2D} phase. Since the hexagonal crystallites exhibited circularly polarized Bragg reflections, it was evident that the observed phase was *three*-dimensional—now identified as BPH^{3D} [D_6^4 ($P6_222$) or D_6^5 ($P6_422$)]. Later work [116] has shown that increasing the electric field causes the reflected intensity to weaken and finally, at a threshold field, to disappear altogether. The platelets remain, however; they are in the BPH^{2D} phase and are detectable in transmission. Decreasing the electric field causes the colored hexagonal BPH^{3D} platelets to reappear. As it turns out, positive dielectric anisotropy is not a requirement: experiments [117] have found three-dimensional hexagonal phases in systems with $\varepsilon_a < 0$.

Later theoretical work by Hornreich and Shtrikman [118], [119] has included the possibility of two- and three-dimensional hexagonal structures for both positive and negative dielectric constant. For $\varepsilon_a > 0$, in addition to their previously predicted BPH^{2D} they predict *two* possible three-dimensional hexagonal phases which they call BPH_a^{3D} and BPH_b^{3D}. For $\varepsilon_a < 0$, BPH^{2D} a two-dimensional phase does not appear, but a single three-dimensional phase, BPH_c^{3D}, does. The results of their calculation are shown in Figure 7.15. So far only one three-dimensional hexagonal phase has been identified for each sign of ε_a. A second hexagonal phase for $\varepsilon_a > 0$ is either not present or has escaped detetection.

Further investigation on the same system [64], [120] has revealed a second field-stabilized phase, called BPX, which has a body-centered tetragonal unit cell with space group D_4^{10} ($I4_122$). This structure can be grown by applying an electric field along the BPI (100) direction, as shown in Figure 7.16. From Kossel diagrams, it is evident that the cubic unit cell first distorts, becoming orthorhombic. Then, above a critical field, the body-centered tetragonal phase locks in. Further details of the transition and of the resulting lattices are found by measurements of the Kossel diagrams. For a discussion of the geometry of BPX, see Pansu [44].

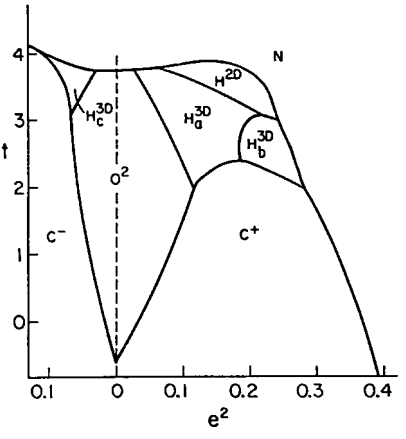

FIGURE 7.15. Theoretical phase diagram showing temperature t versus squared electric field e^2 in reduced units. The phase diagram is for reduced chirality $\kappa = 1.7$; results to the left (right) of the dashed line correspond to $\varepsilon_a < 0$ ($\varepsilon_a > 0$). Shown are the helical phases (C^- or C^+), nematic phase (N), simple cubic phase (O^2), two-dimensional hexagonal phase (BPH^{2D}), and three-dimensional hexagonal phases ($H_a^{3D}, H_b^{3D}, H_c^{3D}$) (from Hornreich and Shtrikman [119]).

7.5.2 *Electrostriction*

For fields which are too small to cause a phase transition, there are two effects. The simplest is to favor a particular orientation of the crystallites without lattice distortion [82]. The second is *electrostriction*, namely a distortion of the cubic blue phase lattice due to applied fields. As in the previous discussion of elastic measurements, this distortion is fundamentally different from that which occurs in a conventional crystal where the lattice is composed of atoms at specific lattice points. In blue phases, it is the lattice of director orientations which does the distorting; the molecules themselves continue to be free to diffuse through this lattice.

A phenomenological theoretical framework for electrostriction in blue phases was first provided by Dmitrienko [121], with additional development

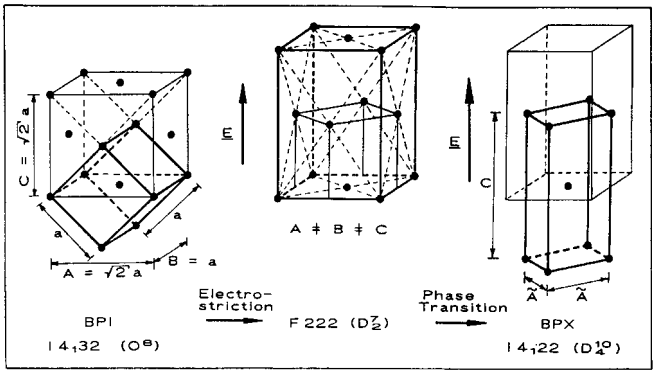

FIGURE 7.16. Transformation of the BPI unit cell into the tetragonal unit cell. From Kitzerow [101].

by Trebin and coworkers [122], [123], [124]. In order to sketch the main ideas, we present this theory first in a simplified, one-dimensional form.

Deformation of a solid object is given by the well-known *strain tensor* of elasticity theory. Let the point originally at location $\mathbf{x}$ be displaced by a small amount $\boldsymbol{\xi}$. The strain tensor u_{ij} is then given by

$$u_{ij} = \frac{1}{2}\left(\frac{\partial \xi_i}{\partial x_j} + \frac{\partial \xi_j}{\partial x_i}\right). \tag{7.13}$$

In order to produce an easily visualized situation, let us suppose that an internal electric field $E_x = E$ produces a compression (or elongation) $\xi_x = \xi$ in the x-direction only. Then $u_{xx} = \partial\xi/\partial x = u$ is the resulting strain and the free energy resulting from this process is [121]:

$$F = F_0 + \tfrac{1}{2}\Lambda u^2 - \tfrac{1}{2}\varepsilon E^2, \tag{7.14}$$

where Λ is an *elastic coefficient* and ε is the *dielectric permittivity*. But ε depends on the strain u and the field E itself, which we describe by expanding ε to lowest relevant orders in u and E:

$$\varepsilon = \varepsilon_0 + bu + \chi E^2. \tag{7.15}$$

The first term, ε_0, represents the unperturbed part of the permittivity; the second term describes the coupling of ε to u, with b an *elasto-optic coefficient*; and the third term describes higher-order terms in E, with χ the *nonlinear dielectric susceptibility*. Substituting (7.15) into (7.14) and retaining only those terms containing u, one gets

$$F = F_0 + \tfrac{1}{2}\Lambda u^2 + \tfrac{1}{2} buE^2. \tag{7.16}$$

Minimizing this equation with respect to u, we can find the strain in terms of the electric field and the phenomenological parameters Λ and b:

$$\begin{aligned} u &= \tfrac{1}{2}\lambda^{-1} bE^2 \\ &= RE^2, \end{aligned} \tag{7.17}$$

where $R = (\Lambda^{-1}b)/2$ is the *electrostriction coefficient*. Thus, in our one-dimensional example, the compression produced on the lattice by an electric field in the same direction is proportional to E^2. The electrostriction coefficient R is the constant of proportionality and its sign determines whether the distortion is compression or elongation. Experiments can produce values for R; it is the task of theory to calculate R from more fundamental quantities.

Of course, an electric field in the x-direction may also cause distortion in the y- and z-directions, therefore a complete theory must take into account the tensor nature of the interactions. This is accomplished by replacing the quantities $E, u, \varepsilon, b, \Lambda, \chi$, and R with, respectively, E_i, u_{ij}, ε_{ij}, b_{ijkl}, Λ_{ijkl}, χ_{ijkl}, and R_{ijkl}, and by replacing (7.17) with

$$u_{ij} = \tfrac{1}{2}\lambda^{-1}_{ijkl} b_{klmp} E_m E_p = R_{ijmp} E_m E_p, \tag{7.18}$$

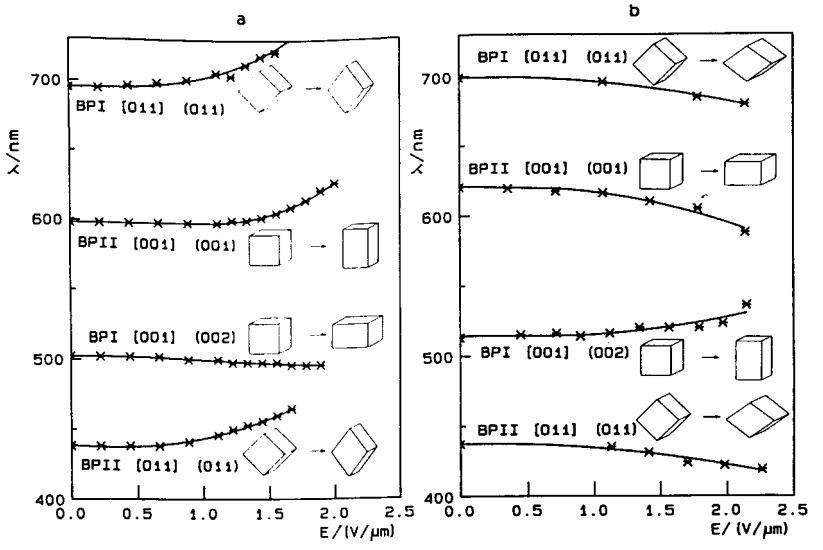

FIGURE 7.17. Bragg wavelengths λ for various crystal planes versus electric field E in BPI and BPII. (a) Negative dielectric anisotropy; (b) positive dielectric anisotropy (from Kitzerow [101]).

where repeated subscripts are summed over. Invoking the symmetry of the lattice greatly simplifies the picture, however, and in the cubic case there are only three R_{ijkl} coefficients: $R_{1111} = R_1$, $R_{1122} = R_2$, and $R_{2323} = R_3/2$.

Electrostriction experiments have been carried out for both BPI and BPII under conditions of both positive and negative dielectric anisotropy [105], [108], [125], [126], [127] using Bragg reflection and Kossel diagram techniques. The essential results are shown in Figure 7.17. Typically, the electrostriction coefficients are $\sim 10^{-15}$–10^{-14} m^2 V^{-2} and, as predicted theoretically, change sign if the dielectric permittivity changes sign. When the volume of the unit cell is unchanged, $R_1 = -2R_2$, as found experimentally [126], [127]. The value R_1/R_3 is positive in BPII, but in BPI is negative and is called *anomalous electrostriction* [122].

Starting with the Landau theory, Trebin and coworkers [122], [124] have calculated the electrostriction coefficients by allowing both the wave vectors and scalar amplitudes of the Fourier components to distort. Good agreement with the data is achieved, except for the case of anomalous electrostriction in BPI. The authors therefore conclude that the explanation for this behavior is beyond the capability of the Landau theory. As described earlier, the same group has also proposed a model of the blue phases incorporating bond-orientational order [45], [46]. However, a calculation of the anomalous electrostriction from this model [123] has had only limited success.

Attention has also been paid to the dynamics of electrostriction. Experiments [128], [129], [130], [131] have shown that, to within instrumental accu-

racy, the relaxation is single exponential, with relaxation times $\tau \sim 10$ s—much longer than refractive index changes in the same material. These times have been fitted to the phenomenological expression [130]:

$$\tau \sim \frac{\gamma L^2}{K}, \tag{7.19}$$

where γ is a viscosity, K is a Frank elastic constant, and the sample size L may be either the thickness of a cell-confined sample or the size of a crystallite. The L^2 behavior of τ has been tested: agreement is fairly good for cell-confined samples but rather poor for crystallites.

7.6 BPIII

We now turn to BPIII, which has been the most enigmatic of the blue phases. Called variously the grey phase [14], the fog phase [70], the blue fog [103], and BPIII [53], the last name seems to have survived. This phase, which is amorphous and not cubic, has been reviewed in preliminary fashion by Crooker [17], Seideman [19], and Wright and Mermin [20], but at the time of these reviews (1989–1990) only the initial experiments had been performed and theoretical attention was just beginning.

7.6.1 Experiment

A review of the experiments until 1989 has been given previously by Crooker [17]; we present only the salient facts here:

- As shown in Figure 7.4, BPIII is the highest temperature blue phase, appearing either between BPII and the isotropic phase, or, at higher chiralities, between BPI and the isotropic phase. Like BPI, but unlike BPII, it is characterized by a temperature range which increases monotonically with increasing chirality.
- The visual appearance of BPIII is foggy, quite unlike the structured appearance of BPI or BPII [14]. Since it appears only at higher chiralities, it is often bluish or grayish in color. At very high chiralities, it may be invisible—indistinguishable from the isotropic phase—to the naked eye. Visually, therefore, BPIII appears to be closer in structure to the isotropic phase than to BPI or BPII.
- Like BPI and BPII, BPIII selectively reflects circularly polarized light [52], [53]. Unlike the cubic blue phases, however, the spectrum is quite broad ($\sim$100 nm) [132]. Also, while BPI and BPII exhibit several Bragg peaks (corresponding to various crystal planes), BPIII exhibits only one peak.
- BPIII exhibits rotatory power, the magnitude of which, in general, decreases with temperature and chirality [133], [134]. At the BPI/BPII–BPIII transition, and at the BPIII–isotropic transition, the rotatory power jumps discontinuously.

- As can be seen from Figure 7.3, there is a small heat capacity peak between BPIII and the cubic blue phases and a much larger peak between BPIII and the isotropic phase. From the heat capacity data, BPIII therefore appears to be closer in structure to BPII than to the isotropic phase, in contrast to the visual appearance.
- As shown in Figure 7.12, measurements of the shear elasticity and the visosity of BPIII show higher values than for the neighboring BPII and isotropic phases [25].
- Electron microscopy of freeze-fractured samples of BPIII have shown a filamentary structure, with details on the order of a tenth of the pitch in the helical phase [135].

The conclusion from this preliminary evidence was that BPIII was a separate phase, thermodynamically distinct from the cubic and isotropic phases, but amorphous and chiral. More recent optical and thermodynamic measurements have proved revealing. Based on a suggestion by Koistinen and Keyes [136] that BPIII and the isotropic phase have the same symmetry, one would expect the BPIII–isotropic coexistence line (see Figure 7.4) to end in a critical point at some higher, unexplored chirality in the temperature–chirality plane. In this respect, the situation is analogous to the liquid–gas coexistence line, which, since liquids and gases have the same symmetry, also ends at a liquid–gas critical point.

Using light scattering [137], [138] and rotatory power techniques [139], Collings and coworkers were able to show that the discontinuities present at low-chirality BPIII–isotropic transitions disappeared at very high chiralities. Figure 7.18 shows the rotatory power data in several chiral–racemic mixtures of the highly chiral liquid crystal CE2 (British Drug House). In these measurements, the chirality is adjusted by mixing n_L moles of the left-handed enantiomer of CE2 with n_R moles of right-handed CE2. The chirality is then proportional to the "chiral mole fraction" $X = (n_L - n_R)/(n_L + n_R)$. Note

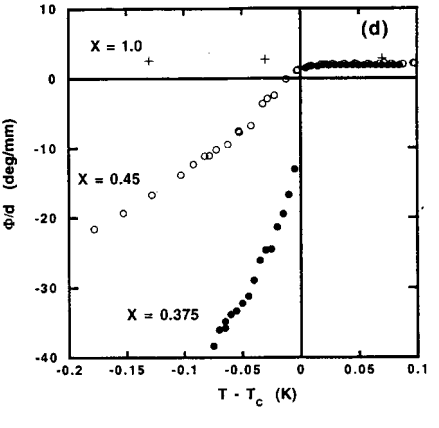

FIGURE 7.18. Rotatory power Φ/d versus temperature T near the BPIII–isotropic transition in three mixtures of varying chirality. The material is a mixture of left- and right-handed enantiomers of CE2 (British Drug House), with chiral mole fraction $X = 0.35, 0.45, 1$. These values bracket the critical point near $X_c = 0.45$ (from Kutjnak et al. [139]).

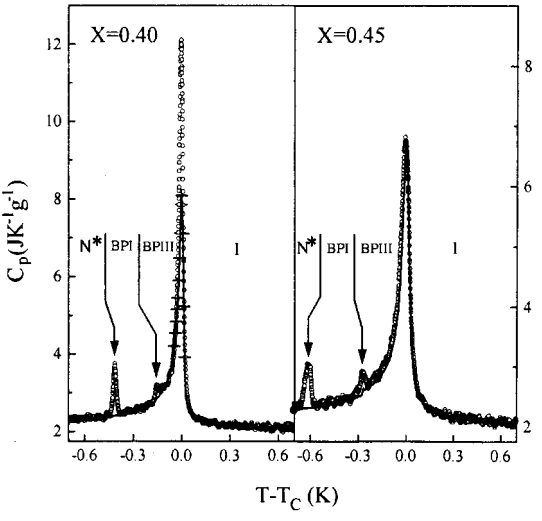

FIGURE 7.19. Nonadiabatic (circles) and adiabatic (smooth curve) calorimetry data for two chiralities of CE2. Peaks appearing only in the nonadiabatic data indicate a first-order transition. The BPIII–isotropic peak evident for $X = 0.40$ has vanished for $X = 0.45$, which is thought to be near the critical point at X_c. The region denoted by + signs indicates phase-shift anomalies in the adiabatic data, which also accompany a first-order transition (from Kutjnak et al. [139]).

that the step in the rotatory power at low chiralities, which is the signature of a first-order transition, disappears at higher chirality.

More evidence for a critical point comes from adiabatic and nonadiabatic scanning calorimetry measurements [138], [139], a comparison of which yields the latent heat effects associated with a first-order phase transition. Figure 7.19 shows data from both techniques for two chiralities of a CE2 sample. The sharp peaks, which are due to the nonabiatic technique only, represent first-order helical–BPI and BPI–BPIII transitions; the BPIII–isotropic peak only shows first-order behavior for $X = 0.40$. Repeated runs for various chiralities establishes that, for this system, $X_c \approx 0.45$. A complete experimental analysis of the rotatory power and calorimetric experiments has been performed by Kutnjak et al. [139], who conclude that the data is consistent with mean field behavior. Since that time, however, new theory has appeared which allows different conclusions.

7.6.2 Theory

As experiments developed a description of BPIII behavior, a number of early models were presented. Up to 1989, these models included the following:

- The *pretransitional fluctuation model* assumed that BPIII is simply a manifestation of pretransitional fluctuations in the isotropic phase at the blue phase–isotropic boundary [3], [4]. This idea was discounted [56] by the fact that the observed BPIII scattering [53] is several orders of magnitude too large for pretransitional fluctuations. In any case, the calorimetry data [26] rule out the pretransitional fluctuation model.
- The *emulsion model* [103] suggested that BPIII is just an emulsion of helical droplets in an isotropic background. This model requires pure materials to have a two-phase region, in violation of thermodynamics, and is also inconsistent with present experiments.
- The *double-twist* model of Hornreich et al. [140] suggests that BPIII is a spaghetti-like tangle of double-twist cylinders (see Figure 7.6), but with a scalar order parameter which dies away in Gaussian-like fashion with increasing distance from the cylinder axis. This model has not been completely discounted to date, and is not in disagreement with present data.
- The *cubic domain model* includes the possibility that BPIII retains local cubic structure, but only over short correlated regions. For these regions, Collings [134] has suggested a BPII-like sc O^2 structure, whereas Belyakov et al. [84] have proposed a BPI-like bcc O^8 structure. Experiments by Yang et al. [141] have shown, however, that BPIII exhibits only a single broad selective reflection peak without any indication of the higher orders expected from a cubic structure. Also, Kitzerow et al. [142] have shown that, for negative dielectric anisotropy, BPIII may be aligned by an electric field, which sharpens and greatly intensifies (by tenfold) the selective reflection peak. Measurements of the line shape and intensity of this peak versus electric field indicate that the coupling between the order parameter Q and the electric field E is proportional to Q^2E^n with n being equal to 2. The cubic model requires $n = 4$ [143], which rules it out; but the double-twist model, for which $n = 2$, is still allowed. In fact, a locally cubic model becomes the double-twist model in the limit of small correlation length, so perhaps the difference between the two is merely a question of the size of the correlation length.
- The *icosahedral model* [144], [145], [146], [147] has been the most analytically tractable so far. Starting from the Landau theory of Hornreich and Shtrikman [32], a structure with reciprocal lattice vectors derived from the vertices of a regular icosahedron is assumed. Using the 12 vertex vectors and the 30 edge vectors of the icosahedron, a structure with a free energy considerably higher than that of, say, the bcc O^5 cubic phase is found. Such a high-energy structure would, of course, be unstable to O^5. If, however, the symmetry is broken by shifting the phases of the edge vectors, the energy can be lowered until the structure is *almost*, but not quite, stable. Nevertheless, the theory may have overlooked some feature, such as higher-order terms, which would make the structure stable. Efforts to verify this model

were attempted by Crooker and coworkers, who searched for, but were unable to find, icosahedral selective reflections [141]. In addition, the electric field experiments mentioned earlier, which ruled out cubic BPIII structures, also ruled out icosahedral structures, for which one expects $n \geq 4$. At present, therefore, due to the lack of experimental and theoretical evidence for the icosahedral structure, attention has turned to other explanations for BPIII.

The notion [136], and accumulating experimental evidence [139], that the the BPIII–isotropic coexistence line might terminate in a critical point has stimulated recent theoretical work by Lubensky and Stark [148]. Letting $\mathbf{Q} = Q_{ij}$ denote the customary order parameter tensor, they assume a new, pseudoscalar order parameter formed from the chiral term in the free energy

$$\langle \psi \rangle = \langle \mathbf{Q} \cdot (\nabla \times \mathbf{Q}) \rangle = \langle \varepsilon_{ijk} Q_{il} \nabla_j Q_{kl} \rangle. \tag{7.20}$$

In a conventional helical structure, $\langle \psi \rangle \sim S^2 q$, where $S = \langle (3\cos^2\theta - 1)/2 \rangle$ is the scalar order parameter and $q = 2\pi/P$; in general, $\langle \psi \rangle$ contains information on both the chirality and the order itself. This new order parameter is discontinuous across the coexistence line, with the discontinuity decreasing to zero at the critical point. In this sense, the BPIII–isotropic transition is analogous to the liquid–gas transition.

Using ψ and $\mathbf{Q}$, a coarse-grained Landau–Ginzburg–Wilson Hamiltonian is written which admits the mixing of the physical variables temperature and chirality to produce the theoretical scaling fields. The critical behavior of this model is then shown to be in the universality class of the three-dimensional Ising model. The authors are also able to derive expressions near the critical point for the light-scattering correlation functions and the rotatory power and claim *qualitative* agreement with the earlier optical experiments of Collings and coworkers [137], [138].

More recently, Anisimov et al. [149] have further exploited the idea of mixing physical variables by *quantitatively* comparing two equations of state—a mean field model and a scaling model—with the heat capacity and optical data of Kutnjak et al. [139]. Writing the scaling fields incorporated in the models as linear combinations of temperature and chirality, they find the mixing for the BPIII–isotropic transition to be more extreme than the analogous liquid–gas transition. Comparing the fits for their two equations of state, the authors claim that the scaling equation of state gives the better fit [see Figure 7.20], which is evidence that this transition does, after all, belong to the same university class as the three-dimensional Ising model.

Finally, we recall the discussion of phase diagrams in Section 7.3.4. In the bond-orientational order model of Trebin et al. [45], [46], only limited success was achieved by modeling BPIII as the O^5 cubic phase with bond-orientational order. Also, in the same authors' fluctuation-dominated model [47], a strong indication of BPIII was impossible to achieve.

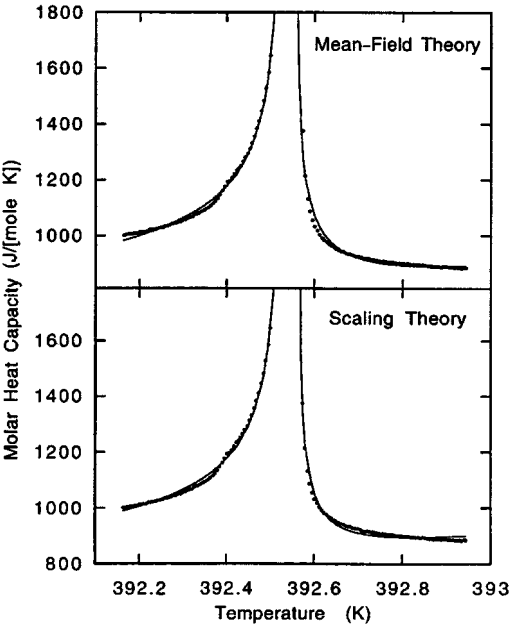

FIGURE 7.20. Molar heat capacity data near the BPIII–isotropic critical point $X = 0.40$. Dots are data; solid lines are fits to the mean-field and scaling theories (from Anisimov et al. [149]).

7.7 Conclusions

Blue phases now seem to be fairly well understood, and a generic picture of the temperature–chirality phase diagram for blue phases has emerged, as shown in Figure 7.21. The survival of BPI and BPIII at high chiralities is well established, as is the existence of a critical point terminating the BPIII–isotropic coexistence line. BPII occupies a temperature region between BPI and BPIII, but only over a limited chirality range. The symmetry of BPI appears to be bcc O^8 ($I4_132$); that of BPII sc O^2 ($P4_232$). Although the short-range structure of BPIII has not yet been strictly determined, it has the same overall symmetry as the isotropic phase, a fact which allows for the appearance of the BPIII–isotropic critical point. One speculation is that BPIII consists of small correlated regions of double twist. Theoretically, production of a phase diagram which brings out all the features of the experimental phase diagram has been a daunting problem and is still ongoing.

Application of small electric fields results in electrostriction of the BPI and BPII lattices. Except for the case of anomalous dispersion in BPI, this behavior has been explained theoretically. Larger fields cause hexagonal and tetragonal phases to be stabilized. The hexagonal phase has received theoretical justification; the tetragonal phase still awaits theoretical treatment.

Finally, we opened this chapter by noting the many surprising ways in which matter can aggregate. Blue phases are only one defect phase to

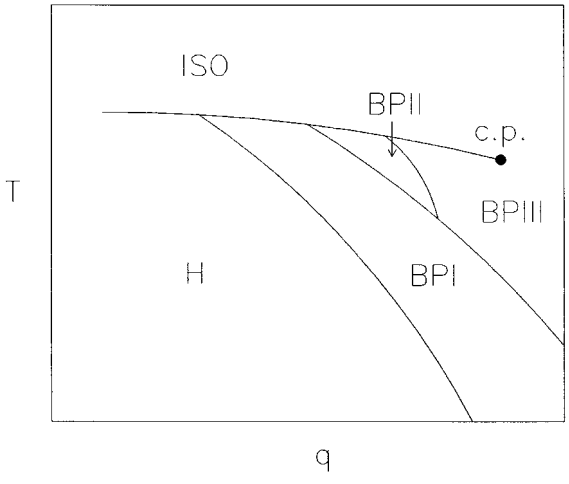

FIGURE 7.21. Generic phase diagram showing temperature T versus chirality q for blue phases. Universal features include the survival of BPI and BPIII, but not BPII, at high chirality and termination of the BPIII–isotropic transition at critical point c.p.

appear in chiral liquid crystals, the other being the twist grain boundary (TGB) phase [150], [151]. Both phases are a result of chirality. Recently Pansu and coworkers [152], [153] have investigated a liquid crystal where the blue phases are adjacent to the TGB phase (no intermediate helical phase), and the blue phase, as revealed by X-rays, has smectic order. This work is very preliminary, but once again nature has presented us with a new, unanticipated chiral structure to try and understand. Thus, research will continue on chiral materials in general and blue phases in particular. As scientists, we can only hope that the end is nowhere near in sight.

Acknowledgments. The author would like to thank the Kent State Physics Department and Liquid Crystal Institute for their hospitality while part of this manuscript was being written. Thanks also to P. Collings and C. Vause for useful discussions on BPIII, and to D. Beck and E. Dodson for a critical reading of the manuscript.

References

[1] P.G. de Gennes and J. Prost, *The Physics of Liquid Crystals*, 2nd ed., Oxford University Press, London, 1993, Sec. 6.5.
[2] P.G. de Gennes, *Mol. Cryst. Liq. Cryst.* **12**, 193 (1971).
[3] S.A. Brazovskii and S.G. Dmitriev, *Zh. Eksp. Teor. Fiz.* **69**, 979 (1975); [*Sov. Phys. JETP* **42**, 497 (1975)].

[4] S.A. Brazovskii and V.M. Filev, *Zh. Eksp. Teor. Fiz.* **75**, 1140 (1978); [*Sov. Phys. JETP* **48**, 573 (1978)].
[5] J.P. Sethna, *Phys. Rev. Lett.* **51**, 2198 (1983).
[6] J.P. Sethna, D.C. Wright, and N.D. Mermin, *Phys. Rev. Lett.* **51**, 467 (1983).
[7] S.A. Brazovskii, *Zh. Eksp. Teor. Fiz.* **68**, 175 (1975); [*Sov. Phys. JETP* **41**, 85 (1975)].
[8] P.P. Crooker, *Mol. Cryst. Liq. Cryst.* **98**, 31 (1983).
[9] J.P. Sethna, in: *Theory and Applications of Liquid Crystals* (edited by J.L. Ericksen and D. Kinderlehrer), Springer-Verlag, New York, 1987, p. 305.
[10] E. Dubois-Violette and B. Pansu, *Mol. Cryst. Liq. Cryst.* **165**, 151 (1988).
[11] W.F. Brinkman and P.E. Cladis, *Physics Today* **35**, 48 (1982).
[12] S. Meiboom, J.P. Sethna, P.W. Anderson, and W.F. Brinkman, *Phys. Rev. Lett.* **46**, 1216 (1981).
[13] See R.M.J. Cotterill, in: *Ordering in Strongly Fluctuation Condensed Matter Systems* (edited by T. Riste), Plenum, New York, 1980 and references therein.
[14] H. Stegemeyer and K. Bergmann, in: *Liquid Crystals of One- and Two-Dimensional Order* (edited by W. Helfrich and G. Heppke), Springer-Verlag, Berlin, 1980, p. 161.
[15] H. Stegemeyer, Th. Blumel, K. Hiltrop, H. Onusseit, and F. Porsch, *Liq. Cryst.* **1**, 1 (1986).
[16] V.A. Belyakov and V.E. Dmitrienko, *Uspekhi Fiz. Nauk* **146**, 369 (1985); [*Sov. Phys. Uspekhi* **28**, 535 (1985)].
[17] P.P. Crooker, *Liq. Cryst.* **5**, 751 (1989).
[18] P.E. Cladis, in: *Theory and Applications of Liquid Crystals* (edited by J.L. Ericksen and D. Kinderlehrer), Springer-Verlag, New York, 1987, p. 73.
[19] T. Seideman, *Rep. Prog. Phys.* **53**, 659 (1990).
[20] D.C. Wright and N.D. Mermin, *Rev. Mod. Phys.* **61**, 385 (1989).
[21] A. Armitage and F.P. Price, *J. Chem. Phys.* **66**, 3414 (1977).
[22] D. Armitage and F.P. Price, *J. Phys.* **36**, C1–133 (1975).
[23] A. Armitage and R.J. Cox, *Mol. Cryst. Liq. Cryst. Lett.* **64**, 41 (1980).
[24] K. Bermann and H. Stegemeyer, *Z. Naturforsch.* **34a**, 251 (1979).
[25] R.N. Kleiman, D.J. Bishop, R. Pindak, and P. Taborek, *Phys. Rev. Lett.* **53**, 2137 (1984).
[26] J. Thoen, *Phys. Rev. A* **37**, 1754 (1987).
[27] G. Voets, H. Martin, and W. van Dael, *Liq. Cryst.* **5**, 871 (1989).
[28] K. Tanimoto, P.P. Crooker, and G.C. Koch, *Phys. Rev. A* **32**, 1893 (1985).
[29] J.D. Miller, P.R. Battle, P.J. Collings, D.K. Yang, and P.P. Crooker, *Phys. Rev. A* **35**, 3959 (1987).
[30] M.B. Atkinson and P.J. Collings, *Mol. Cryst. Liq. Cryst.* **136**, 141 (1986).
[31] D.K. Yang and P.P. Crooker, *Phys. Rev. A* **35**, 4419 (1987).
[32] R.M. Hornreich and S. Shtrikman, *J. Phys.* **41**, 335 (1980); **42**, 367(E) (1981).
[33] R.M. Hornreich and S. Shtrikman, in: *Liquid Crystals of One- and Two-Dimensional Order* (edited by W. Helfrich and G. Heppke), Springer-Verlag, Berlin, 1980, p. 185.
[34] R.M. Hornreich and S. Shtrikman, *Phys. Rev. A* **24**, 635 (1981).
[35] R.M. Hornreich and S. Shtrikman, *Phys. Lett.* **84A**, 20 (1981).
[36] H. Grebel, R.M. Hornreich, and S. Shtrikman, *Phys. Rev. A* **28**, 1114 (1983).
[37] H. Grebel, R.M. Hornreich, and S. Shtrikman, *Phys. Rev. A* **30**, 3264 (1984).
[38] H. Kleinert and K. Maki, *Fortschr. Phys.* **29**, 219 (1981).

[39] R.M. Hornreich and S. Shtrikman, *Mol. Cryst. Liq. Cryst.* **165**, 183 (1988).
[40] L. Longa, D. Monselesan, and H.-R. Trebin, *Liq. Cryst.* **5**, 889 (1989).
[41] J.P. Sethna, *Phys. Rev. B* **31**, 6278 (1985).
[42] S. Meiboom, M. Sammon, and D. Berreman, *Phys. Rev. A* **28**, 3553 (1983).
[43] S. Meiboom, M. Sammon, and W.F. Brinkman, *Phys. Rev. A* **27**, 438 (1983).
[44] B. Pansu, *J. Phys. II France* **5**, 573 (1995).
[45] L. Longa and H.-R. Trebin, *Phys. Rev. Lett.* **71**, 2757 (1993).
[46] L. Longa and H.-R. Trebin, *Liq. Cryst.* **21**, 243 (1996).
[47] J. Englert, L. Longa, H. Stark, and H.-R. Trebin, *Phys. Rev. Lett.* **81**, 1457 (1998).
[48] K. Bergmann and H. Stegemeyer, *Ber. Bunsenges. Phys. Chem.* **82**, 1309 (1978).
[49] K. Bergmann, P. Pollmann, G. Scherer, and H. Stegemeyer, *Z. Naturforsch.* **34a**, 253 (1979).
[50] K. Bergmann and H. Stegemeyer, *Z. Naturforsch.* **34a**, 1031 (1979).
[51] H. Stegemeyer, *Phys. Lett.* **79A**, 425 (1980).
[52] S. Meiboom and M. Sammon, *Phys. Rev. Lett.* **44**, 882 (1980).
[53] S. Meiboom and M. Sammon, *Phys. Rev. A* **24**, 468 (1981).
[54] D.L. Johnson, J.H. Flack, and P.P. Crooker, *Phys. Rev. Lett.* **45**, 641 (1980).
[55] R.M. Hornreich and S. Shtrikman, *Phys. Lett.* **82A**, 345 (1981).
[56] R.M. Hornreich and S. Shtrikman, *Phys. Rev. A* **28**, 1791 (1983); **28**, 3669(E) (1983).
[57] V.A. Belyakov, V.E. Dmitrenko, and S.M. Osadchii, *Zh. Eksp. Teor. Fiz.* **83**, 585 (1982); [*Sov. Phys. JETP* **56**, 322 (1982)].
[58] K. Tanimoto and P.P. Crooker, *Phys. Rev. A* **29**, 1566 (1984).
[59] J.W. Gorman Jr. and P.P. Crooker, *Phys. Rev. A* **31**, 910 (1985).
[60] J.L. Birman, R.M. Hornreich, and S. Shtrikman, *Phys. Rev. A* **39**, 1590 (1989).
[61] J.H. Flack, P.P. Crooker, and R.C. Svoboda, *Phys. Rev. A* **26**, 723 (1982).
[62] J.W. Gorman Jr. and P.P. Crooker, *Phys. Rev. A* **31**, 910 (1985).
[63] P. Pieranski, E. Dubois-Violette, F. Rohten, and L. Strelecki, *J. Phys.* **42**, 53 (1981).
[64] P.E. Cladis, T. Garel, and P. Pieranski, *Phys. Rev. Lett.* **57**, 2841 (1986).
[65] P. Pieranski and P.E. Cladis, *Phys. Rev. A* **35**, 355 (1987).
[66] B. Jérôme, P. Pieranski, V. Godec, G. Haran, and C. Germain, *J. Phys. France* **49**, 837 (1988).
[67] R.J. Miller and H.F. Gleeson, *Phys. Rev. E* **52**, 5011 (1995).
[68] R.J. Miller and H.F. Gleeson, *J. Phys. II France* **6**, 909 (1996).
[69] R.J. Miller, H.F. Gleeson, and J.E. Lydon, *Phys. Rev. Lett.* **77**, 857 (1996).
[70] M. Marcus, *J. Phys.* **42**, 61 (1981).
[71] M. Marcus, *Phys. Rev. A* **25**, 2272 (1982).
[72] M.J. Costello, S. Meiboom, and M. Sammon, *Phys. Rev. A* **29**, 2957 (1984).
[73] D.W. Berreman, S. Meiboom, J.A. Zasadzinski, *Phys. Rev. Lett.* **57**, 1737 (1986).
[74] H. Onusseit and H. Stegemeyer, *Z. Naturforsch.* **36a**, 1083 (1981).
[75] H. Onusseit and H. Stegemeyer, *J. Cryst. Growth* **61**, 409 (1983).
[76] H. Onusseit and H. Stegemeyer, *Z. Naturforsch.* **38a**, 1114 (1983).
[77] Th. Blümel and H. Stegemeyer, *J. Cryst. Growth* **66**, 163 (1984).
[78] Th. Blümel and H. Stegemeyer, *Z. Naturforsch.* **40a**, 260 (1985).
[79] R. Barbet-Massin, P.E. Cladis, and P. Pieranski, *Phys. Rev. A* **30**, 1161 (1984).

[80] P. Pieranski, R. Barbet-Massin, and P.E. Cladis, *Phys. Rev. A* **31**, 3912 (1985).
[81] P. Pieranski, P.E. Cladis, and R. Barbet-Massin, *J. Phys.* **47**, 129 (1986).
[82] P. Pieranski, P.E. Cladis, T. Garel, and R. Barbet-Massin, *J. Phys. (Paris)* **47**, 139 (1986).
[83] T.K. Brog and P.J. Collings, *Mol. Cryst. Liq. Cryst.* **60**, 65 (1980).
[84] V.A. Belyakov, E.I. Demikhov, V.E. Dmitrienko, and V.K. Dolganov, *Zh. Eksp. Teor. Fiz.* **89**, 2035 (1985); [*Sov. Phys. JETP* **62**, 1173 (1986)].
[85] P.J. Collings, *Mol. Cryst. Liq. Cryst.* **113**, 277 (1984).
[86] M.B. Atkinson and P.J. Collings, *Mol. Cryst. Liq. Cryst.* **136**, 141 (1986).
[87] J. Ennis, J.E. Wyse, and P.J. Collings, *Liq. Cryst.* **5**, 861 (1989).
[88] D. Bensimon, E. Domany, and S. Shtrikman, *Phys. Rev. A* **28**, 427 (1983).
[89] T. Yamada and E. Fukada, *Jap. J. Appl. Phys.* **12**, 68 (1973).
[90] P.H. Keyes and D.B. Ajgaonkar, *Phys. Lett.* **64A**, 298 (1977).
[91] H. Stegemeyer and P. Pollmann, *Mol. Cryst. Liq. Cryst.* **82**, 123 (1982).
[92] T. Harada and P.P. Crooker, *Phys. Rev. Lett.* **34**, 1259 (1975).
[93] D.S. Mahler, P.H. Keyes, and W.B. Daniels, *Phys. Rev. Lett.* **36**, 491 (1976).
[94] P.H. Keyes and C.C. Yang, *J. Phys. Colloq.* **40**, C3–376 (1979).
[95] P.P. Crooker and W.G. Laidlaw, *Phys. Rev. A* **21**, 2174 (1980).
[96] N. Clark, S.T. Vohra, and M.A. Handschy, *Phys. Rev. Lett.* **52**, 57 (1984).
[97] P.E. Cladis, P. Pieranski, and M. Joanicot, *Phys. Rev. Lett.* **52**, 542 (1984).
[98] A.I. Feldman, P.P. Crooker, and L.M. Goh, *Phys. Rev. A* **35**, 842 (1987).
[99] W. Kuczynski and H. Stegemeyer, *Naturwiss.* **67**, 310 (1980).
[100] Th. Blümel and H. Stegemeyer, *Liq. Cryst.* **3**, 195 (1988).
[101] H.-S. Kitzerow, *Mol. Cryst. Liq. Cryst.* **207**, 981 (1991).
[102] D. Lubin and R.M. Hornreich, *Phys. Rev. A* **36**, 849 (1987).
[103] P.L. Finn and P.E. Cladis, *Mol. Cryst. Liq. Cryst.* **84**, 159 (1982).
[104] F. Porsch, H. Stegemeyer, and K. Hiltrop, *Z. Naturforsch.* **39a**, 475 (1984).
[105] H. Stegemeyer and F. Porsch, *Phys. Rev. A* **30**, 3369 (1984).
[106] F. Porsch and H. Stegemeyer, *Chem. Phys. Lett.* **125**, 319 (1986).
[107] H. Stegemeyer and B. Spier, *Chem. Phys. Lett.* **133**, 176 (1987).
[108] G. Heppke, M. Krumrey, and F. Oestreicher, *Mol. Cryst. Liq. Cryst.* **99**, 99 (1983).
[109] G. Heppke, H.-S. Kitzerow, and M. Krumrey, *Mol. Cryst. Liq. Cryst.* **150b**, 265 (1987).
[110] P. Pieranski, P.E. Cladis, and R. Barbet-Massin, *Liq. Cryst.* **5**, 829 (1989).
[111] R.M. Hornreich, M. Kugler, and S. Shtrikman, *Phys. Rev. Lett.* **54**, 2099 (1985).
[112] R.M. Hornreich, M. Kugler, and S. Shtrikman, *J. Phys. Colloque* **C3**, C3–47 (1985).
[113] F. Porsch and H. Stegemeyer, *Liq. Cryst.* **2**, 395 (1987).
[114] N.R. Chen and J.T. Ho, *Phys. Rev. A* **35**, 4886 (1987).
[115] P. Pieranski, P.E. Cladis, and R. Barbet-Massin, *J. Phys. Lett.* **46**, 973 (1985).
[116] M. Jorand and P. Pieranski, *J. Phys. (Paris)* **48**, 1197 (1987).
[117] G. Heppke, B. Jérôme, H.-S. Kitzerow, and P. Pieranski, *Liq. Cryst.* **5**, 813 (1989).
[118] R.M. Hornreich and S. Shtrikman, *Liq. Cryst.* **5**, 777 (1989).
[119] R.M. Hornreich and S. Shtrikman, *Phys. Rev. A* **41**, 1978 (1990).
[120] P. Pieranski and P.E. Cladis, *Phys. Rev. A* **35**, 355 (1987).
[121] V.E. Dmitrienko, *Liq. Cryst.* **5**, 847 (1989).

[122] H. Stark and H.-R. Trebin, *Phys Rev. A* **44**, 2752 (1991).
[123] L. Longa, M. Zelazna, H.-R. Trebin, and J. Moscicki, *Phys. Rev. E* **53**, 6067 (1996).
[124] M. Zelazna, L. Longa, H.-R. Trebin, and H. Stark, *Phys. Rev. E* **57**, 6711 (1998).
[125] G. Heppke, H.-S. Kitzerow, and M. Krumrey, *Mol. Cryst. Liq. Cryst. Lett.* **1**, 117 (1985).
[126] G. Heppke, B. Jérôme, H.-S. Kitzerow, and P. Pieranski, *J. Phys. France* **50**, 549 (1989).
[127] G. Heppke, B. Jérôme, H.-S. Kitzerow, and P. Pieranski, *J. Phys. France* **50**, 2991 (1989).
[128] H.F. Gleeson and H.J. Coles, *Liq. Cryst.* **5**, 917 (1989).
[129] H.-S. Kitzerow, P.P. Crooker, S.L. Kwok, and G. Heppke, *J. Phys. France* **51**, 1303 (1990).
[130] H.-S. Kitzerow, P.P. Crooker, S.L. Kwok, J. Xu, and G. Heppke, *Phys. Rev. A* **6**, 3442 (1990).
[131] H.-S. Kitzerow, P.P. Crooker, J. Rand, J. Xu, and G. Heppke, *J. Phys. II France* **2**, 179 (1992).
[132] E.l. Demikhov, V.K. Dolganov, and S.P. Krylova, *Pis'ma Zh. Eksp. Teor. Fiz.* **42**, 15 (1985); [*JETP Lett.* **42**, 15 (1985)].
[133] E.I Demikhov and V.K. Dolganov, *Sov. Phys. JETP Lett.* **38**, 445 (1983).
[134] P.J. Collings, *Phys. Rev. A* **30**, 1990 (1984).
[135] J.A.N. Zasadzinski, S. Meiboom, M.J. Sammon, and D.W. Berreman, *Phys. Rev. Lett.* **57**, 364 (1986).
[136] E.P. Koistenen and P.H. Keyes, *Phys. Rev. Lett.* **74**, 4460 (1995).
[137] J.B. Becker and P.J. Collings, *Mol. Cryst. Liq. Cryst.* **265**, 163 (1995).
[138] Z. Kutnjak, C.W. Garland, J.L. Passmore, and P.J. Collings, *Phys. Rev. Lett.* **74**, 4859 (1995).
[139] Z. Kutnjak, C.W. Garland, C.G. Schatz, P.J. Collings, C.J. Booth, and J.W. Goodby, *Phys. Rev. E* **53**, 4955 (1996).
[140] R.M. Hornreich, M. Kugler, and S. Shtrikman, *Phys. Rev. Lett.* **48**, 1404 (1982).
[141] D.K. Yang, P.P. Crooker, and K. Tanimoto, *Phys. Rev. Lett.* **61**, 2685 (1988).
[142] H.-S. Kitzerow, P.P. Crooker, and G. Heppke, *Phys. Rev. Lett.* **67**, 2151 (1991).
[143] R.M. Hornreich, *Phys. Rev. Lett.* **67**, 2155 (1991).
[144] R.M. Hornreich and S. Shtrikman, *Phys. Rev. Lett.* **56**, 1723 (1986).
[145] R.M. Hornreich and S. Shtrikman, *Phys. Lett. A* **115**, 451 (1986).
[146] D.S. Rokhsar and J.P. Sethna, *Phys. Rev. Lett.* **56**, 1727 (1986).
[147] V.M. Filev, *Pis'ma Zh. Eksp. Teor. Fiz.* **43**, 523 (1986); [*JETP Lett.* **43**, 677 (1986)].
[148] T.C. Lubensky and H. Stark, *Phys. Rev. E* **53**, 714 (1996).
[149] M.A. Anisimov, V.A. Agayan, and P.J. Collings, *Phys. Rev. E* **57**, 582 (1998).
[150] S.R. Renn and T.C. Lubensky, *Phys. Rev. A* **38**, 2132 (1988).
[151] J.W. Goodby, M.A. Waugh, S.M. Stein, E. Chin, R. Pindak, and J.S. Patel, *Nature* **337**, 449 (1989).
[152] B. Pansu, M.H. Li, and H.T. Nguyen, *J. Phys. II France* **7**, 751 (1997).
[153] B. Pansu, M.H. Li, and H.T. Nguyen, *European Phys. J. B* **2**, 143 (1998).